Recent Advances in Layered Two-dimensional Ferroelectrics from Material to Device

Shenmao Lin, Geyang Zhang, Qinglin Lai, Jun Fu, Wenguang Zhu, and Hualing Zeng*

With the advent of the post Moore era, modern electronics require further device miniaturization of all electronic components, particularly ferroelectric memories, due to the need for massive data storage. This demand stimulates the exploration of robust switchable ferroelectric polarizations at the atomic scale. In this scenario, van der Waals ferroelectrics have recently gained increasing attention because of their stable layered structure at nanometer thickness, offering the opportunity to realize two-dimensional ferroelectricity that is long-sought in conventional thin film ferroelectrics. In this review, recent advancements are summarized in layered ferroelectrics with highlights of the fundamentals of intrinsic two-dimensional ferroelectricity, the emergence of artificial stacking ferroelectricity, and related protype devices with exotic functions. In addition, the unique polarization control in van der Waals ferroelectrics is discussed. Although great challenges remain unsolved, these studies undoubtedly advance the integration of 2D ferroelectrics in electronics.

1. Introduction

The study of ferroelectricity has gone through more than a hundred years with rich progress achieved that has made great contributions to modern electronics.[1–7] Thin-film ferroelectric oxides represented by $PbTiO_3$, $BaTiO_3$, and HfO_2 (or $Hf_{0.5}Zr_{0.5}O_2$) have been integrated in silicon-based electronics, showing technical practicality in nonvolatile memories via devices such as ferroelectric diodes,[8,9] ferroelectric transistors,[10,11] and ferroelectric tunneling junctions.[12–14] As electronics enter the post

S. Lin, G. Zhang, Q. Lai, J. Fu, W. Zhu, H. Zeng
International Center for Quantum Design of Functional Materials (ICQD)
Hefei National Research Center for Physical Sciences at the Microscale
University of Science and Technology of China
Hefei 230026, China
E-mail: hlzeng@ustc.edu.cn
S. Lin, G. Zhang, Q. Lai, J. Fu, W. Zhu, H. Zeng
Key Laboratory of Strongly Coupled Quantum Matter Physics
Department of Physics
Chinese Academy of Sciences
University of Science and Technology of China
Hefei, Anhui 230026, China
S. Lin, G. Zhang, Q. Lai, J. Fu, W. Zhu, H. Zeng
Hefei National Laboratory
University of Science and Technology of China
Hefei 230088, China

The ORCID identification number(s) for the author(s) of this article can be found under https://doi.org/10.1002/adfm.202304139

DOI: 10.1002/adfm.202304139

Moore era, the sizes of ultracompact electronic devices are approaching down to several nanometers and even subnanometers.[15–17] Therefore, to meet the raised standard of device miniaturization, there is growing interest in exploring nanoscale ferroelectricity in ferroelectric materials and device communities. For instance, switchable electric polarizations have recently been demonstrated in atomically thin freestanding perovskite membranes[18] and a few nanometers thick HfO_2.[19] In addition to the unremitting efforts to realize ultrathin oxide ferroelectric films, another potential route is to seek robust ferroelectricity at the 2D limit in van der Waals (vdW) materials, which benefits from their innate layer structure with a stable chemical environment and weak packing interactions at the interface. These features not only help to overcome challenges such as surface dangling bonds and giant depolarization fields in conventional ferroelectrics but also open the venue to study the unprecedented interplay between ferroelectricity and metallicity[20,21] and even superconductivity.[22]

The ferroelectric properties in vdW materials can be divided into out-of-plane or in-plane ferroelectricity that is perpendicular or parallel to the 2D plane, respectively.[23,24] In this review, we mainly restrict our discussions to 2D materials with out-of-plane ferroelectricity while leaving the in-plane case briefly mentioned. One reason lies in that 2D materials with out-of-plane ferroelectricity might have greater potential values from the perspective of technical applications. For example, 2D out-of-plane ferroelectricity can be effectively integrated into various vdW heterostructures as a nonvolatile tuning knob for optical,[25–28] electrical,[29–35] and magnetic properties.[36,37] Therefore, the device potential and function tunability of vdW heterostructures will be substantially broadened. Second, it should be noted that it is relatively difficult to obtain out-of-plane ferroelectricity in vdW materials. For in-plane ferroelectricity in vdW materials, the direction of the electric polarization is within the 2D plane. The crystal lattice theoretically maintains near-infinite periodic expansions in this direction. Therefore, the 2D in-plane ferroelectricity might resemble that observed in conventional bulk materials and will be hardly affected by the critical size effect. However, in the out-of-plane direction, the dimensionality decreases, and the material itself becomes a limited system. To maintain stable out-of-plane ferroelectric polarization in a single atomic layer, the structural stability of the vdW material needs to be considered.

**ADVANCED
SCIENCE NEWS**

www.advancedsciencenews.com

**ADVANCED
FUNCTIONAL
MATERIALS**

www.afm-journal.de

Merely pure discoveries on 2D ferroelectricity can contribute importantly to enriching the study of the family of vdW materials with findings on new structures, exotic phases, and extraordinary mechanisms.[21,38–42]

To date, explorations of 2D out-of-plane ferroelectrics have mainly been conducted along two lines. One focus is on the search for intrinsic 2D monolayer crystals that satisfy spatial inversion symmetry breaking in the out-of-plane direction. The ferroelectric polarizations mainly stem from the off-center displacement of specific atoms in their unit cells with the formation of switchable electric dipoles. Stable out-of-plane ferroelectricity and lattice structure benefit from the significant anisotropy along the same direction in 2D systems. Representative materials include $CuInP_2S_6$ (CIPS),[23,43] α-In_2Se_3,[39,40] Bi_2O_2Se,[44,45] and d1T-$MoTe_2$.[46] On the other hand, the innate layer degree of freedom in vdW materials allows the realization of artificial ferroelectricity at the atomic scale by stacking two or multiple 2D monolayers. Switchable out-of-plane ferroelectric polarizations are induced by interlayer compensation charges. Since the monolayer crystals used in stacking can vary from insulators (hexagonal boron nitride, abbreviated as h–BN)[47–49] to semiconductors (ReS_2)[50] and even to semimetals (graphene)[51,52] without constraints on lattice spatial inversion symmetry, these discoveries greatly expand the family of 2D ferroelectrics and lead to the emergence of so-called sliding ferroelectricity (or stacking ferroelectricity).

In view of the rapid progress in 2D ferroelectrics, we summarize recent advancements from material realization to device application. The review is organized as follows: The fundamentals of intrinsic vdW ferroelectrics are first introduced with a focus on out-of-plane ferroelectricity and its unique polarization couplings in 2D systems. We next discuss the emergence of artificial 2D stacking ferroelectricity from theoretical predictions to experimental realizations. Based on intrinsic and artificial 2D out-of-plane ferroelectricity, we review related protype devices with exotic functions, such as ferroelectric field-effect transistors, ferroelectric semiconductor field-effect transistors, ferroelectric channel transistors, and ferroelectric tunneling junction devices. Finally, we provide an outlook of the challenges and opportunities in the study of 2D ferroelectrics.

2. Intrinsic 2D vdW Ferroelectrics

Since graphene was successfully exfoliated in 2004, many 2D materials have emerged with exotic physical properties, such as h-BN, the family of transition metal dichalcogenides (TMDs), and group-IV monochalcogenides. Despite the enormous growth in 2D material science, ferroelectricity was theoretically predicted and experimentally confirmed only recently. Due to their superior nature, including clean vdW interfaces, robustness against depolarization fields, and clean surfaces with no dangling bonds, 2D ferroelectrics are now considered to provide an opportunity in developing ultrathin memory devices. Here, we summarize the development and fundamentals of intrinsic 2D ferroelectrics.

2.1. In-Plane Ferroelectric Polarization

In 2016, several theoretical works predicted stable in-plane spontaneous polarization in monolayer group-IV monochalcogenides MX (M = Ge, Sn; X = S, Se). Bulk MX monochalcogenides adopt an orthorhombic (*Pnma*) crystal structure similar to black phosphorus at room temperature, which maintains inversion symmetry.[53,54] The ferroelectricity of MX is induced by the relative in-plane displacement of anions and cations, which breaks the space inversion symmetry. Chang et al. prepared atomically thin SnTe by using the molecular beam epitaxy technique.[24] They observed the formation of a domain structure and band bending induced by spontaneous polarization through scanning tunnelling microscopy (STM) and scanning tunneling spectroscopy (STS) and manipulated the polarization through the STM tip. The above evidence demonstrates the existence of stable in-plane spontaneous polarization in atomic-thin SnTe down to a 1–unit cell limit. The ferroelectric transition temperature T_c of the 1–unit cell SnTe film is as high as 270 K, which is much higher than the 98 K of the bulk material. In addition, the 2-4-unit cell SnTe film has a higher T_c and room-temperature ferroelectricity. The T_c enhancement in ultrathin SnTe films is ascribed to the formation of γ-SnTe.[55] Analogously, robust in-plane ferroelectricity in monolayer SnSe and few-layer SnS was observed.[56,57] Moreover, an inverse piezoelectric effect is observed in SnS films with an odd number of layers, manifested as spontaneous rippling of the film along the polarization direction. In addition, an electric-field-induced reversible antiferroelectric to ferroelectric transition at room temperature in layered α-GeSe was also reported.[58]

In addition to MX, SbN, and BiP with a phosphorus-like structure are also predicted to be room-temperature 2D ferroelectric materials.[59] The in-plane polarization of SbN can reach up to $7.81 \times 10^{-10}\ C\ m^{-1}$. Based on the controlled ferroelectric domains, polarized 2D ferroelectrics show the potential to fabricate devices, such as nonvolatile ferroelectric random-access memory and in-plane ferroelectric tunneling junctions.

2.2. Out-of-Plane Ferroelectric Polarization

Out-of-plane spontaneous ferroelectric polarization was most intensively discussed in the transition metal thiophosphate (TMTP) family, including CIPS, $CuInP_2Se_6$, and $AgBiP_2Se_6$.[23,43,60–62] To date, the ferroelectricity in some TMTPs has been experimentally confirmed, and CIPS is recognized to be one of their most representative. The lattice structure of CIPS is shown in **Figure 1**a. The octahedral cages formed by sulfur atoms are filled with metal cations Cu and In and P−P pairs in the octahedral voids, and a complete unit cell of CIPS is made up of two adjacent monolayers in which the sites of Cu and P-P pairs exchange. Spontaneous polarization of CIPS originates from the atomic position deviation of Cu cations in each single layer, which breaks the lattice inversion symmetry. In 2015, Belianinov et al. first reported the existence of room temperature ferroelectric polarization in layered CIPS with the observation of ferroelectric domains and hysteresis loops in CIPS with a thickness greater than 100 nm.[43] This work inspired further exploration of ultrathin ferroelectric materials.[63,64] For example, Liu et al. reported room-temperature out-of-plane ferroelectricity in ultrathin CIPS with a film thickness down to 4 nm (Figure 1b).[23]

As a room-temperature 2D ferroelectric material, CIPS has a series of unique properties, including the coexistence of negative
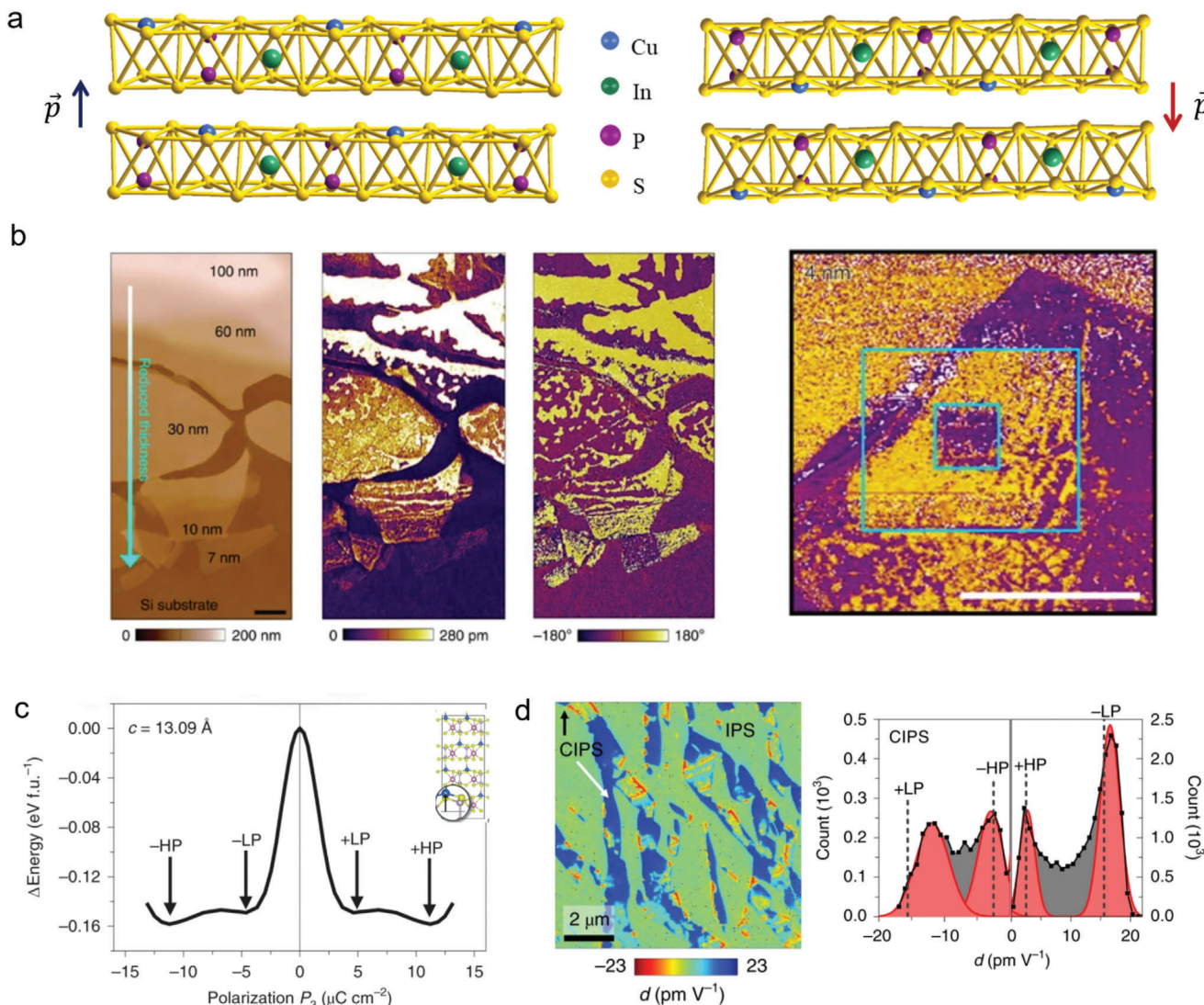
**ADVANCED
SCIENCE NEWS**

www.advancedsciencenews.com

**ADVANCED
FUNCTIONAL
MATERIALS**

www.afm-journal.de

Figure 1. a) Side views of the crystal structure of CIPS with two opposite polarization directions. The polarization direction is indicated by the arrow. b) AFM topography, PFM amplitude, and PFM phase of CIPS ranging from 100 to 7 nm thick (left). The PFM phase image of 4 nm thick CIPS with written box-in-box patterns (right). Scale bar, 1 µm.[23] c) The energy change curve as a function of polarization from the zero-displacement Cu site at a fixed lattice parameter of 13.09 Å. The curve exhibits four local energy minima along the z-axis and two minima in each of the polarization directions along the z-axis. The inset shows the relaxed structure of CIPS according to the HP phase.[38] d) Map of quantified piezoelectric constant measured by PFM (left). The color scale depicts the magnitude and direction of the measured piezoresponse. Histogram of the CIPS phase measurements fitted with Gaussian functions with four distinct maxima (right). Dotted lines depict the theoretically predicted values of the four polarization states.[38] Reproduced under the terms of the CC–BY license.[23] Copyright 2016, The Authors, published by Springer Nature. Reproduced with permission.[38] Copyright 2019, Springer Nature.

longitudinal piezoelectric coefficients,[23,65] ionic conduction,[66] and atypical polarization switching,[67] among which the most attractive is the existence of a quadruple-well potential.[38] Unlike the classic Landau–Ginzburg–Devonshire double-well potential, which has two minima corresponding to two polarization states, layered CIPS has a quadruple-well potential for uniaxial Cu-ion displacements. The tunable quadruple-well model was demonstrated theoretically and experimentally by Brehm et al. The layered structure leads to a second stable Cu site within the vdW gap, which possesses a small energy barrier difference, thus forming interlayer bonds with S atoms from adjacent layers. As a result, four local energy minima exist along the z-axis (see Figure 1c), with two called the low-polarization (LP) and the others termed the higher-polarization (HP) phases. Calculated with density functional theory (DFT), the Cu-ion displacements of LP and HP are ≈1.62 Å and ≈2.25 Å, respectively, and the polarization values of ±HP (± 11.26 µC cm^{-2}) are more than twice those in ±LP (± 4.93 µC cm^{-2}). By piezoelectric force microscopy (PFM), the existence of quadruple-well potential was demonstrated. Strong piezoelectric responses with four individual maxima in the histogram were observed from CIPS at room temperature, as shown in Figure 1d.

In other family members of TMTP, such as $CuCrP_2S_6$ and $CuInP_2Se_6$, out-of-plane ferroelectricity and anti-ferroelectricity

were also experimentally demonstrated. Lai et al. predicted that ferromagnetism coexists with electric-field-driving ferroelectricity in ultrathin $CuCrP_2S_6$ and revealed out-of-plane ferroelectric polarization at room temperature in few-layer $CuCrP_2S_6$ (approximately 13 nm thick).[68] Dziaugys et al. reported that the antiferroelectric and ferroelectric phases coexist in $CuInP_2Se_6$. The maximum piezoelectric response was found at the domain walls (approximately four times larger if compared to that from domains), which is different from the minimum piezoelectric response found at the domain walls in ferroelectrics.[69] The phenomenon of multiphase coexistence in $CuInP_2Se_6$ extends the study of domain wall electronics.

In parallel, there is gaining interest in exploring intrinsic ferroelectricity in group VI TMDs such as MX_2 (M = Mo, W and X = S, Se) due to their abundant properties. In 2014, Shirodkar and Waghmare theoretically predicted that $1T$-MoS_2 has out-of-plane ferroelectric polarization.[70] The unstable K_3 modes due to the degeneracy of the Fermi surface and strong electron-phonon coupling cause trimerization distortion of Mo atoms in monolayer $1T$-MoS_2. As a result, the centrosymmetric 1T phase transitions to a distorted 1T ($d1T$) phase with broken inversion symmetry. This theoretical analysis is also applicable to other TMDs, such as $MoSe_2$, WS_2, and WSe_2, providing theoretical support for ferroelectricity in TMDs. However, room-temperature OOP ferroelectricity has only been observed in monolayer d$1T$-$MoTe_2$ thus far.[46,71] The ferroelectricity in d$1T$-$MoTe_2$ results from the relative atomic displacements of Mo atoms and Te atoms.

2.3. Intercorrelated in-Plane and out-of-Plane Ferroelectric Polarization

Another hallmark in vdW ferroelectrics is the discovery of semiconducting In_2Se_3 with unique intercorrelated in-plane and out-of-plane ferroelectric polarizations. In 2017, Ding et al. predicted the existence of room-temperature ferroelectricity in In_2Se_3 and other III_2-VI_3 vdW materials, possessing both in-plane and out-of-plane spontaneous polarization.[39] The crystal structure of In_2Se_3 is shown in **Figure 2**a. A quintuple layer (QL) of In_2Se_3 has five atomic layers, which are covalently bonded and arranged alternately in the sequence of Se-In-Se-In-Se atomic layers. The QLs stack vertically via weak vdW interactions, and different stacking orders lead to different In_2Se_3 phases. As the most stable phase at room temperature, α-In_2Se_3 has two stacking orders, namely, the hexahedral (2H) structure and the rhombohedral (3R) structure. The horizontal and vertical distances between the central Se atomic layer and the two adjacent In atomic layers are obviously different, which leads to the breaking of the spatial inversion symmetry. The atomic-resolution scanning transmission electron microscopy (STEM) image of 3R α-In_2Se_3 is shown in Figure 2c, demonstrating the layered noncentrosymmetric lattice structure. When the central Se atomic layer shifts, it changes the horizontal and vertical distances with neighbouring In atoms, resulting in simultaneous in-plane and out-of-plane polarization switching (Figure 2b). Zhou et al. first experimentally demonstrated ferroelectricity in 3R α-In_2Se_3, and the out-of-plane polarization is potentially switchable in films down to approximately 10 nm thick.[72] In 2018, the coupling between in-plane and out-of-plane ferroelectricity in 3R α-In_2Se_3 was experimentally confirmed.[40,41] For example, Cui et al. electrically wrote two box patterns with opposite voltages in a 6 nm sample via PFM in the out-of-plane direction and observed that the in-plane electric polarization changes simultaneously.[40] In the same year, Xue et al. also demonstrated the phenomenon of intercorrelated in-plane and out-of-plane polarization in 2H α-In_2Se_3.[73] Moreover, the piezoresponse hysteresis loop of monolayer 2H α-In_2Se_3 reveals that room-temperature ferroelectricity still persists in the monolayer limit ($\approx$ 1.2 nm) (Figure 2e).

At the early stage, there are very few vdW ferroelectrics with the special property of intercorrelated in-plane and out-of-plane electric polarizations. To expand 2D ferroelectrics with similar electric dipole locking in α-In_2Se_3, Hu et al. experimentally demonstrated intercorrelated in-plane and out-of-plane polarizations in β-InSe nanoflakes at room temperature.[74] Simultaneous in-plane and out-of-plane polarization switching with bias was observed in 10 nm thick β-InSe. In addition to In_2Se_3 and InSe, similar ferroelectric behavior has also been observed in layered $CuCrS_2$ by Xu et al.[75] recently with high T_c at 700 K. In layered $CuCrS_2$, the Cu atoms occupy tetrahedral sites in the interstices between the two CrS_2 layers, and the interlayer spacing between the Cu layer and the two adjacent CrS_2 layers is unequal, which breaks the inversion symmetry. As Cu atoms shift between sites, the relative lateral and vertical displacement of the positive charge center leads to intercorrelated in-plane and out-of-plane polarization, as observed in $CuCrS_2$.

Based on the coupled ferroelectricity, the out-of-plane electric polarization can be switched via an in-plane electric field, and vice versa.[40,41] This intriguing polarization field control allows the development of multidirectional and efficient data writing and reading strategies in ferroelectric memory devices based on α-In_2Se_3-related 2D ferroelectrics.[76,77] Together with their semiconducting nature, electrical nonvolatility can be directly integrated into α-In_2Se_3-based field-effect transistor devices.[32,78,79] In general, this remarkable property might have great potential for the design of advanced 2D electronic devices, which will be discussed in the following section.

3. Stacking Ferroelectricity in Multilayer vdW Materials

With the rapid progress in 2D ferroelectrics, a fact that cannot be ignored is that only a few layered materials have been experimentally verified to have intrinsic out-of-plane ferroelectricity. To expand this family, the innate layer degrees of freedom in vdW materials are utilized to artificially produce the so-called interlayer sliding ferroelectricity by stacking two or multiple monolayers with a twist angle or a relative lateral shift. The inherent mechanism is distinct from that established in conventional ferroelectrics, which is induced by ion displacement. Since sliding ferroelectricity can be achieved even with nonpolar monolayers, it greatly opens up new possibilities for the design and realization of 2D ferroelectrics.

3.1. Theoretical predictions

The earliest prediction of sliding ferroelectricity was proposed in 2017, revealing the universal existence of out-of-plane ferroelectricity in 2D bilayer materials.[42] The theoretical model started
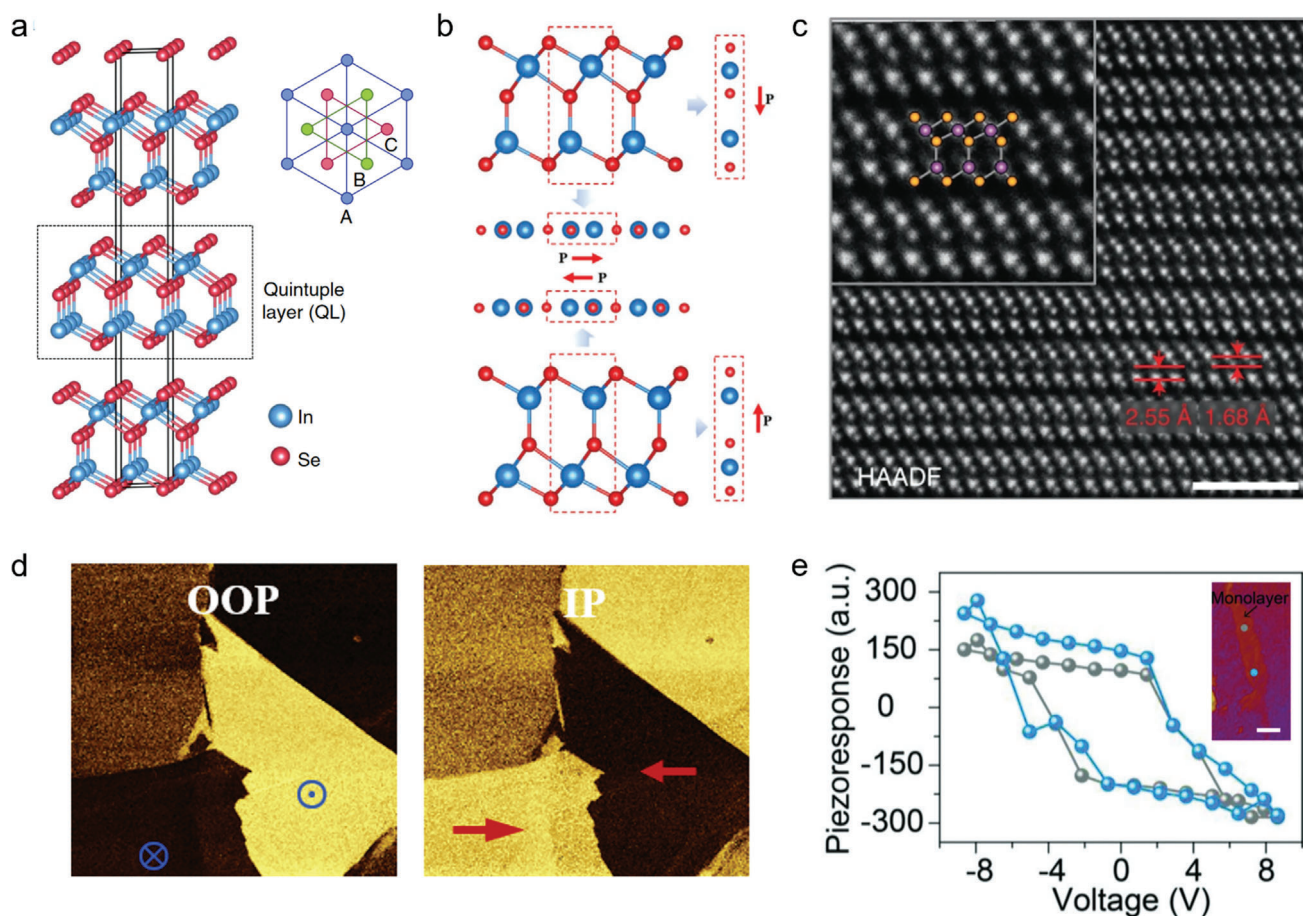
**ADVANCED
SCIENCE NEWS**

www.advancedsciencenews.com

**ADVANCED
FUNCTIONAL
MATERIALS**

www.afm-journal.de

Figure 2. a) Three-dimensional crystal structure of layered In_2Se_3 (left). The black dashed square indicates a QL. Vertical top view of the system (right). Each atomic layer in QL contains only one type of element, and the atoms are arranged in one of the triangular lattices A, B, or C.[39] b) Side views of one QL α-In_2Se_3 with two opposite polarizations. Projection of the atoms into the c and a (or b) axes indicates the principle of intercorrelated ferroelectricity in α-In_2Se_3. Red arrows indicate the directions of the electric polarization.[77] c) Scanning transmission electron microscopy high–angle annular dark–field (STEM-HAADF) image of the α-In_2Se_3 crystal. Inset shows the magnified image overlaid with calculated results. Scale bar, 2 nm.[122] d) PFM phase images of OOP (left) and IP (right) spontaneous polarization in α- In_2Se_3. e) Ferroelectric hysteresis loops of 2H α- In_2Se_3 crystals in the monolayer limit. Inset shows the typical monolayer α- In_2Se_3 flake. Curves show the color guides from the corresponding spots in the inset. Scale bar, 300 nm.[73] Reproduced under the terms of the CC–BY license. [39] Copyright 2017, The Authors, published by Springer Nature.Reproduced with permission.[73] Copyright 2018, Wiley–VCH. Reproduced the terms of the CC–BY license.[77] Copyright 2020, The Authors, published by Wiley–VCH. Reproduced with permission.[122] Copyright 2022, Springer Nature.

with bilayer h-BN, as shown in **Figure 3**a. A natural bulk h-BN usually has an antiparallel (AA′) stacking configuration, where the N (B) atoms in each layer completely overlap with the B (N) atoms in the adjacent layer. This stacking is centrosymmetric and does not support the occurrence of out-of-plane electric polarization. Upon a relative lateral shift or twist, the AA′ structure can be changed into either AA or AB/BA stacking order (see Figure 3b). For AA stacking, the two BN monolayers are stacked by mirror symmetry without rotation and are long assumed to be an unstable structure. For AB stacked bilayer BN, the N atoms in the upper layer face the six-ring centers in the lower layer, while the upper layer B atoms sit exactly on the N atoms in the lower layer. This stacking order leads to the breaking of the inversion symmetry, and significant electric polarizations stem from the net charge transfer between layers. Furthermore, the AB and BA stacking configurations are associated by mirror symmetry. Therefore, opposite interlayer electric polarizations can be established along

the out-of-plane direction, and polarization reversal can be realized via lateral sliding along the armchair direction (as indicated by the red arrows in Figure 3a), which meets the standard of ferroelectrics. Similarly, by twisting with a small angle, as shown in Figure 3b, periodic ferroelectric domains can be created in the form of moiré patterns containing AB, BA, and AA stacking orders at different regions separated by domain walls.[80]

According to the above theoretical model, the charge compensation between two monolayers leads to the emergence of 2D out-of-plane ferroelectricity. Such unconventional ferroelectricity can probably be extended to many other bilayer vdW materials with 2D honeycomb lattices, such as few-layer graphene, AlN, MoS_2, and GaSe. To date, many 2D materials can be endowed with sliding ferroelectricity by precisely controlling the stacking order with subtle lateral shifting or twisting. In a very recent theoretical study, all the possible bilayer stacking ferroelectricity was summarized in all 80 layer groups by performing systematic
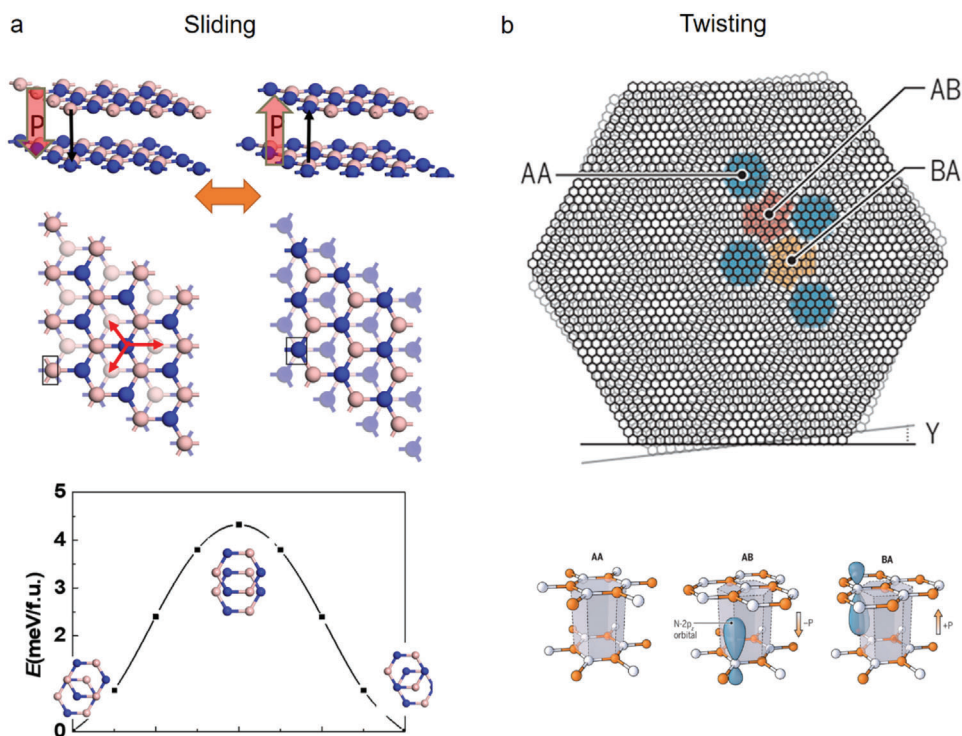
**ADVANCED
SCIENCE NEWS**

www.advancedsciencenews.com

**ADVANCED
FUNCTIONAL
MATERIALS**

www.afm-journal.de

Figure 3. Artificial ferroelectricity in vdW layered materials. a) The theoretical model of sliding ferroelectricity in bilayer BN via interlayer sliding, where the red arrows denote the polarization directions.[125] b) Periodic moiré patterns containing AA regions separated by AB and BA domains in twisted bilayer BN.[80] Reproduced with permission.[80] Copyright 2021, The American Association for the Advancement of Science. Reproduced with permission.[125] Copyright 2021, The National Academy of Sciences (NAS).

group theory analysis.[81] These predictions of stacking ferroelectricity lay a solid foundation for the realization of a large number of bilayer ferroelectrics.[42,81–83]

### 3.2. Experimental Realizations of Twisting Ferroelectricity

Since twisted bilayer 2D materials have been most intensively studied in recent years, we first review the progress of sliding ferroelectricity realized by twisting. Taking graphene as the most representative example, monolayer graphene is a kind of 2D semimetal. When twisting two graphene layers with a magic angle, the electronic structure can be strongly modified with the rise of many novel phenomena. In 2020, Zheng et al. reported the interlayer switchable ferroelectricity observed in a Bernal-stacked bilayer graphene[51] device with a moiré superlattice pattern, as shown in **Figure 4**a. The transport measurement in the twisted graphene device showed significant hysteresis between the forward and backwards bottom gate voltage scanning, which suggested the existence of electrical polarization in the out-of-plane direction. By measuring the remnant polarization, the polarization density in twisted bilayer graphene was approximately 0.18 $\mu C\ cm^{-2}$. Later, in 2022, Niu et al. designed an optimized device with a similar twisting manner and observed giant ferroelectric polarization[52] up to 5 pC m^{-1}.

Compared with twisted bilayer graphene, the twisted homo or heterobilayer of TMDs might offer a broader diversity for electronics,[84–87] which benefits from their moderate bandgaps.

In 2H-stacked bilayer TMDs, the upper layer metal atoms are vertically aligned with the bottom layer chalcogen atoms, which follows global inversion symmetry. Similarly, the centrosymmetric 2H phase of bilayer TMDs can be broken by stacking two monolayers with a small twist angle. In 2020, Weston et al. reported the atomic structure and electronic properties in twisted WS_2 and MoS_2 with atomic-resolved STEM and conductive atomicforce microscopy (AFM).[88] By using the tear-and-stamp transfer technique, WS_2 and MoS_2 homo and heterobilayers with parallel (P) or antiparallel (AP) alignment can be fabricated at various twisting angles ($\theta < 3°$), where perfect P alignment would lead to a 3R stacking order and AP alignment would produce a 2H stacking phase. A small angular deviation from the perfect P or AP alignment would result in a periodic moiré pattern. For imperfect P or AP orientations, lattice reconstruction reconstructed the moiré pattern into lattice domains, which can be clearly observed from the diffraction contrast in low-magnification STEM. In addition, Wang et al. characterized the ferroelectric properties in similar triangular domains with the PFM technique on a small-angle twisted bilayer $MoSe_2$.[89] Weston et al. reported the observation of ferroelectric domain networks in bilayer MoS_2 and their correlation with the interlayer twist angle by combining electric transport measurements.[90]

As predicted, the artificial ferroelectricity can be applicable to insulating 2D materials such as h-BN. In 2021, to prove this,[47,48] Stern et al. stacked two 3 nm thick h-BN thin layers with a small twisting angle on a conducting substrate. By Kelvin probe force microscopy (KPFM), they observed oppositely polarized domains
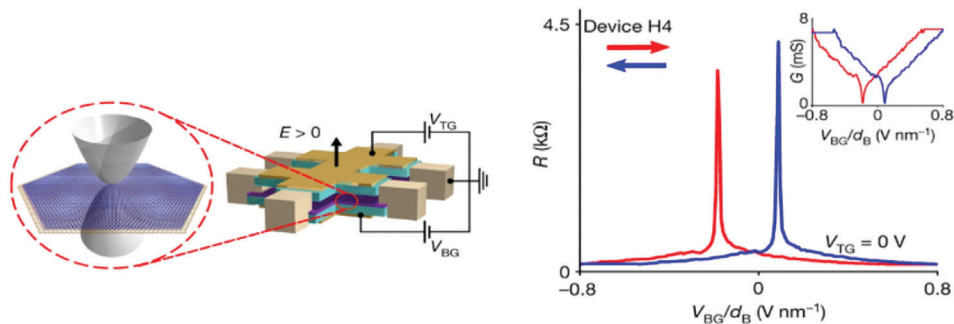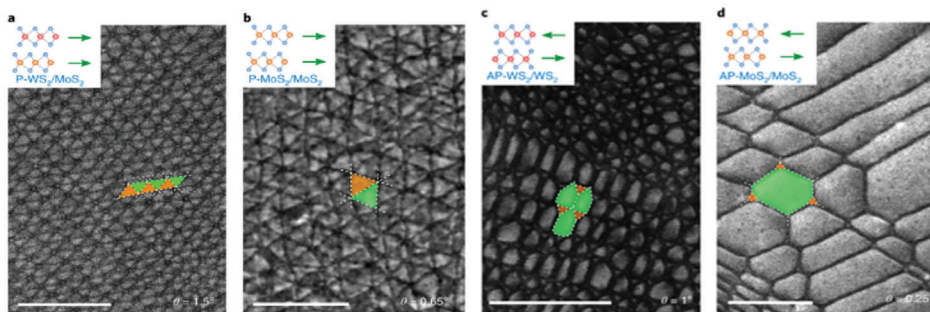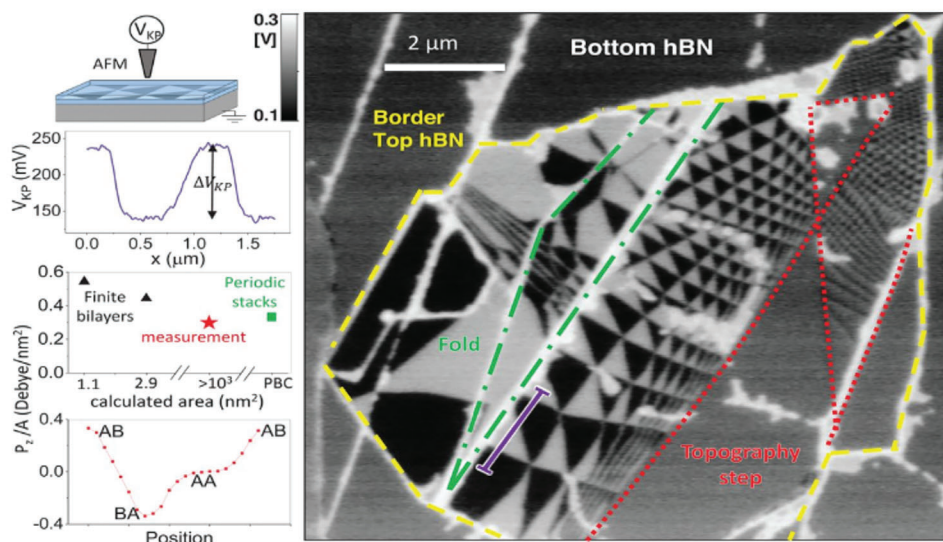
Figure 4. Twisted ferroelectricity in 2D Moiré lattices. a) BN-encapsulated bilayer device with a schematic diagram of the BLG/BN moiré superlattice pattern and four-probe resistance for a hysteretic device.[51] b) Images of lattice domains with diffraction contrast at low magnification, and colors highlight different types of domains.[88] c) Direct measurement of oppositely polarized domains in two twisted 3 nm thick h-BN thin layers by AFM operated in KPFM.[49] Reproduced with permission.[49] Copyright 2021, The American Association for the Advancement of Science. Reproduced with permission.[51] Copyright 2020, Springer Nature. Reproduced with permission.[88] Copyright 2020, Springer Nature.
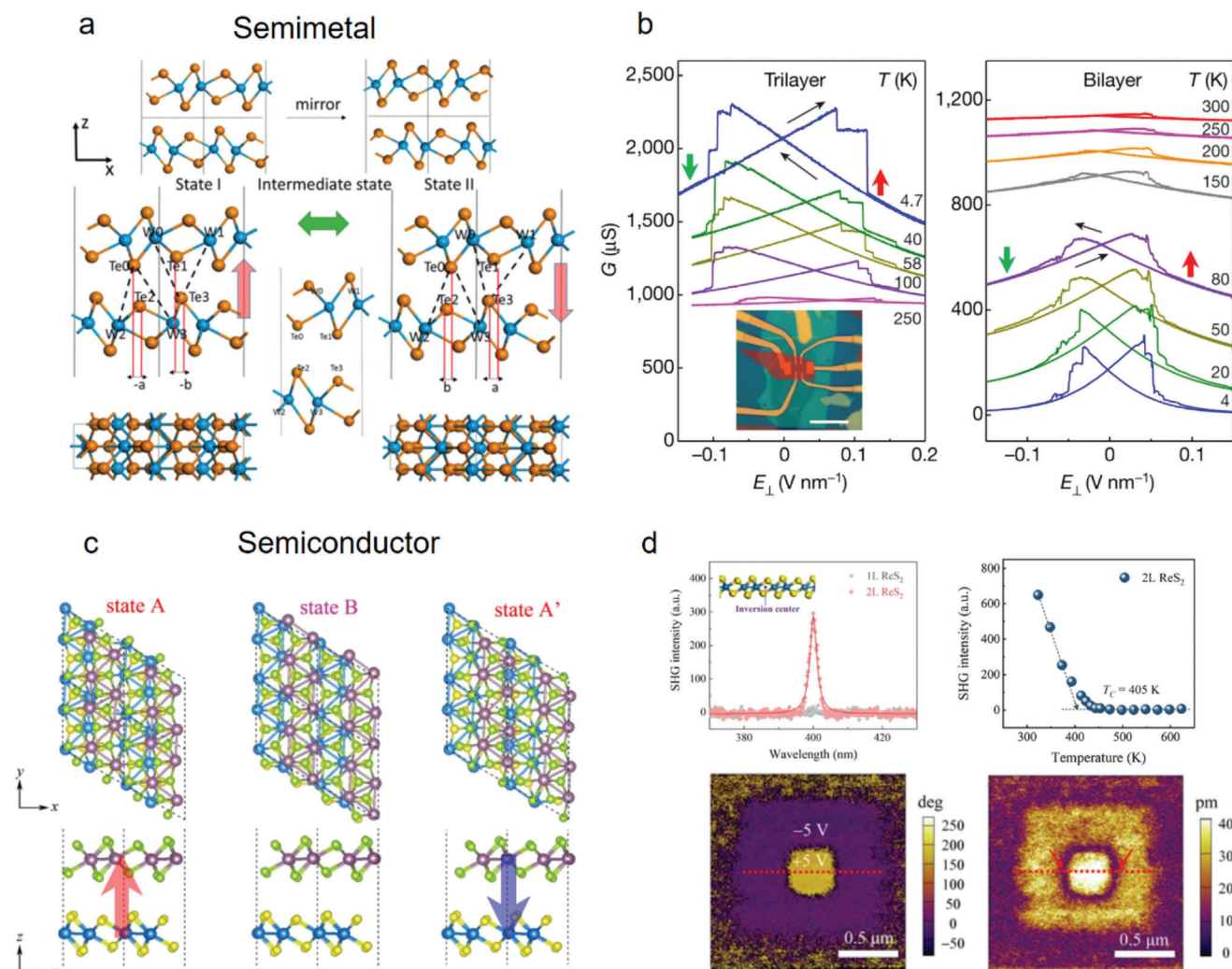
**ADVANCED
SCIENCE NEWS**

www.advancedsciencenews.com

**ADVANCED
FUNCTIONAL
MATERIALS**

www.afm-journal.de

Figure 5. Sliding ferroelectricity in vdW multilayers. a) Geometric structure of state I and state II of bilayer WTe_2, where the red arrows denote the polarization directions.[93] b) Conductance G of trilayer and bilayer devices, which are sensitive to the out-of-plane electric field $E_\perp$.[21] c) Two energy-degenerate ferroelectric structures (states A and A′) and a high-symmetry nonpolar structure (state B) of bilayer ReS_2. The red and blue arrows indicate the opposite polarization direction.[50] d) SHG spectra obtained from monolayer and bilayer ReS_2. Temperature dependence of the SHG intensity of bilayer ReS_2. PFM phase and amplitude images for four layers of ReS_2 on graphene.[50] Reproduced with permission.[21] Copyright 2018, Springer Nature. Reproduced with permission.[50] Copyright 2022, American Physical Society. Reproduced with permission.[93] Copyright 2018, American Chemical Society.

stemming correspondingly from the AB and BA stacking regions, as shown in Figure 4c.[49] Since domain walls can be locally pushed through mechanical disturbance and electrical disturbance at the nanoscale,[91,92] the local stacking order in stacking bilayers can be changed in the same way. In this work, a reversible polarization switch was accompanied by relatively moving the interface by tip punching. The dynamic flipping of the polarization was visualized in the KPFM images, which fitted well with the results from DFT calculations.

3.3. Experimental Realizations of Sliding Ferroelectricity

The earliest experimental discovery on stacking ferroelectricity can be dated back to 2018. Fei et al. conducted vertical electric

transport measurements on WTe_2 thin layers, which was actually the first experimental verification of sliding ferroelectricity.[21] They designed a device with WTe_2 thin layers sandwiched by two h-BN dielectric sheets, as shown in **Figure 5**b. Using few-layer graphene as gate electrodes, they observed bistable conducting states and clear switchable hysteretic behavior in bilayer and trilayer devices. In contrast, such hysteresis loops were not observed in monolayer WTe_2. However, the origin of sliding ferroelectricity from multilayer WTe_2 was unclarified at that time. Later in the same year, Yang et al. revealed the mechanism by first-principles calculations, and the theoretical results were consistent with the experimental observations.[93] The geometric structures of bilayer WTe_2 were classified into state I and state II, as shown in Figure 5a. Interlayer sliding leads to the transition from state I to state II but with reversed vertical

**ADVANCED
SCIENCE NEWS**

www.advancedsciencenews.com

**ADVANCED
FUNCTIONAL
MATERIALS**

www.afm-journal.de

polarization. The nonequivalence between the upper and lower layers therefore gives rise to uncompensated charge transfer and vertical polarization. Similarly, the mechanism of sliding ferroelectric bilayer WTe_2 is applicable to multilayers.

Semiconducting vdW materials with moderate bandgaps might have broader application prospects. In this sense, it is of great significance to explore the existence of sliding ferroelectricity in 2D semiconductors aside from metals, semimetals and insulators. In a combined theoretical and experimental study by Wan et al., sliding ferroelectricity was verified in multilayer semiconducting ReS_2.[50] In bilayer ReS_2, upon different lateral slidings, as shown in Figure 5c, there are two energy-degenerate ferroelectric structures (states A and A′) and a high-symmetry nonpolar structure (state B). First-principles DFT calculations revealed that the vertical polarization and interlayer translation in multilayer ReS_2 are strongly coupled, which hints at the existence of switchable ferroelectric polarizations. By using PFM and second harmonic generation (SHG) measurements, out-of-plane ferroelectricity in ultrathin 1T′-ReS_2 with layer number N ≥ 2 was confirmed, as shown in Figure 5d, via clear evidence from the observation of the ferroelectric to paraelectric phase transition and artificially created domain walls. In other TMD family members, such as MoS_2, WS_2, and related heterostructures, sliding ferroelectricity has also been identified recently. In 2022, Rogée et al. synthesized untwisted, commensurate, and epitaxial MoS_2/WS_2 heterobilayers by chemical vapour deposition and observed unexpected out-of-plane ferroelectricity and piezoelectricity. Their DFT calculations showed that interface inversion symmetry breaking and interlayer sliding could produce such ferroelectricity without invoking twisting angles.[94] In multilayer 3R-MoS_2, Meng et al. designed dual-gate field-effect transistors with different film thicknesses and observed abnormal intermediate polarization states.[95]

4. Device Applications with 2D Ferroelectrics

With the reversibility and long-term retention of electric polarizations, ferroelectrics have played an important role in nonvolatile memory devices. In ultrathin devices, oxide ferroelectrics usually have difficulty in reducing the leakage current arising from outstanding interfacial issues. Benefitting from the inert and saturated surfaces in vdW ferroelectrics, the above device interface properties can be optimized with the establishment of sharp band edges and the minimization of interfacial traps.[96] Thus, 2D ferroelectrics based devices might have superior electric performance, such as higher on/off ratio, higher carrier mobility, and enhanced photovoltaic response. Here, we introduce several representative architectures of 2D ferroelectrics based nonvolatile memories and optoelectronic devices.

4.1. Ferroelectric Field-Effect Transistors (FeFETs)

FeFET utilizes ferroelectric materials as the gate dielectric layer to tune the resistance of the channel. With the retention of electric polarizations, the on or off state can be maintained, thus

functioning as nonvolatile memories. In 2019, Wan et al.[31] reported a 2D FeFET based on atomically thin α-In_2Se_3. As shown in **Figure 6**a, ultrathin α-In_2Se_3 layers, graphene, and heavily doped SiO_2/Si served as the top-gate dielectric, conducting channel, and back gate, respectively. Atomically thin h-BN was used to improve the device interface properties and enhance the intrinsic conductivity of graphene. Figure 6b shows the optical image of the FeFET device, in which the thickness of the α-In_2Se_3 layers is down to 2.6 nm. By applying the top-gate voltage (V_{TG}), the electric dipoles in α-In_2Se_3 were electrically polarized in the out-of-plane direction, which would significantly dope graphene with different types of carriers via the induced screening charges, leading to a shift in the Fermi level (E_F) of graphene and modulation of its conductivity. To be used as a nonvolatile memory device, the stable states of upwards and downwards are supposed to be able to represent the logic bits. As shown in Figure 6c, the authors used heavily doped p-type graphene as the conducting channel, whose initial E_F is far from its Dirac point. The resistance contrast $\frac{\Delta R}{R}$ (defined as $|\frac{R_{P\uparrow}-R_{P\downarrow}}{R_{P\uparrow}+R_{P\downarrow}}|$, where $R_{P\uparrow}$ and $R_{P\downarrow}$ represent resistances with upward and downward electric polarization, respectively) was successfully increased from 1% (neutral graphene) to 58.5%. In addition, after ±3 V polarizing, the residual resistances were still distinguishable in a time span of 1000 s. After over 10^5 cycles of repeated writing and erasing, the performance of the device remained stable. In addition to using gapless graphene as the conducting channel, Huang et al.[34] proposed a dual-gated heterostructure FeFET with MoS_2 as the channel and CIPS as the ferroelectric gating layer in 2020. With the insertion of h-BN and the dual-gated coupling device configuration, the device shows a high on/off ratio (10^7), low off-state current (10^{-13} A), and a relatively long retention time (10^4 s). Other FeFETs using similar CIPS/MoS_2 structures with an on/off ratio over 10^4 have also been reported.[29]

Although these pioneering works successfully show the practicability of 2D FeFETs with a remarkable on/off ratio up to 10^7, as a kind of memory device, the retention time is not long enough at that stage. To overcome this issue, Wang et al.[97] demonstrated an all-vdW FeFET in 2021 with a 10-year memory retention. Their device utilized a heterostructure of CIPS/graphene/h-BN/MoS_2. Along with the h-BN dielectric, the graphene served as an internal gate, which minimized the depolarization in the device. Therefore, the device not only shows an on/off ratio greater than 10^7 but also has a 10-year memory retention and endurance of more than 10^4 cycles.

4.2. Ferroelectric Semiconductor Field-Effect Transistors (FeS-FETs)

Different from the FeFET, which essentially lies on the ferroelectric gating layer, the FeS-FET integrates the electrical nonvolatility directly by using a semiconducting ferroelectric material as the channel, as shown in Figure 6d. In 2019, Si et al.[32] proposed an FeS-FET using α-In_2Se_3 as the channel with passivation provided by Al_2O_3 to enhance performance (Figure 6e). Owing to the semiconducting feature of ferroelectric In_2Se_3, there is intricate interplay between the mobile charges and the electric polarizations.
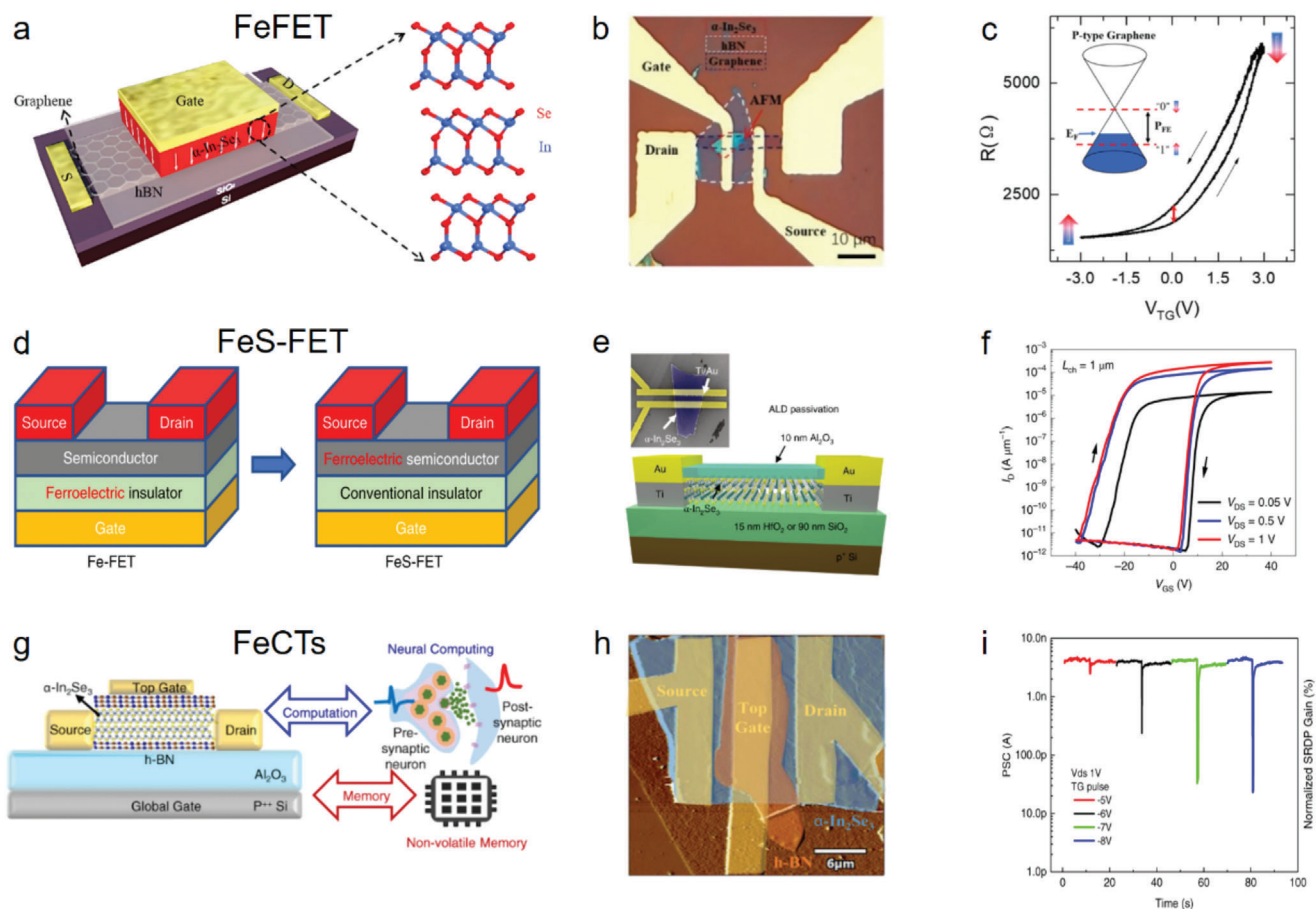
ADVANCED
SCIENCE NEWS

www.advancedsciencenews.com

ADVANCED
FUNCTIONAL
MATERIALS

www.afm-journal.de

Figure 6. Nonvolatile memories based on 2D α-In$_2$Se$_3$. a) Schematic diagram and b) optical image of the FeFET with a vertically stacked graphene/h-BN/α-In$_2$Se$_3$ structure. The white arrows in the concept diagram indicate the direction of electric polarization.[31] c) The hysteretic ferroelectric gating in p-FeFET. The upwards and downwards arrows represent the bistable ferroelectric polarizations in α-In$_2$Se$_3$. The small bidirectional red arrows in the hysteresis loop indicate the resistance states for the remnant electric polarizations. The inset shows the initial Fermi level of heavily doped p-type graphene. The red dashed lines indicate the final E_F after the electric polarization of α-In$_2$Se$_3$ thin layers.[31] d) Schematic diagram of the comparison between FeFET and FeS-FET. In FeFETs, the ferroelectric insulator serves as a gate dielectric, while in FeS-FETs, the ferroelectric semiconductor serves as the channel.[32] e) Schematic of the experimental α-In$_2$Se$_3$ FeS-FET with ALD passivation and a false-color SEM image of a fabricated α-In$_2$Se$_3$ FeS-FET.[32] f) The I$_D$-V$_{GS}$ characteristics of an α-In$_2$Se$_3$ FeS-FET with 90 nm SiO$_2$ as the gate dielectric.[32] g) Schematic diagram and h) false-color AFM image of α-In$_2$Se$_3$ FeCTs, which integrate memory and computing functions.[79] i) A typical neural STP simulation under short negative spikes.[79] Reproduced with permission.[31] Copyright 2019, Wiley–VCH. Reproduced with permission.[32] Copyright 2019, Springer Nature. Reproduced the terms of the CC–BY license.[79] Copyright 2021, The Authors, published by Springer Nature.

In the FeS-FET, mobile charges are allowed to accumulate at both the bottom and top surface of the channel, depending on the relative alignments of the conduction or valence band edges and the E_F that are controlled by the electric polarizations. The drain current is therefore modulated. In addition, since the electric field intensity across a semiconductor is strongly affected by the effective oxide thickness (EOT) of the insulating dielectrics, the polarization in α-In$_2$Se$_3$ can be further tuned by controlling the EOT. In the high-EOT condition, the electric field across the semiconductor is not strong enough to penetrate the channel, and only local polarization occurs near the oxide/semiconductor interface. In the low-EOT condition, the electric field is strong enough to trigger full polarization switching in the ferroelectric semiconductor. Therefore, combining these features, the FeS-FET device achieved a high on/off ratio (10^8), a large memory window, and a maximum drain current of 862 µAµm^{-1} (Figure 6f). An-

other FeS-FET employing the cointegration of α-In$_2$Se$_3$ and CIPS was also reported.[35] The dipole coupling of CIPS and α-In$_2$Se$_3$ leads to enhanced polarization and thus reaches a larger memory window.

4.3. Ferroelectric Channel Transistors (FeCTs)

With the exponential increase in memory capacity, the bandwidth for data transfer between the central processing unit and memory becomes a bottleneck, which is known as the Von Neumann bottleneck. Memristors offer a solution of being directly integrated on the processor chip to overcome this bottleneck.[98] Thus, ferroelectric memristors have recently been widely studied in neural computing.

**ADVANCED
SCIENCE NEWS**

www.advancedsciencenews.com

**ADVANCED
FUNCTIONAL
MATERIALS**

www.afm-journal.de

In 2020, Wang et al.[79] proposed FeCTs based on α-In_2Se_3, which integrates the functions of nonvolatile memory and neural computation. As shown in Figure 6g, the device used a 40 nm thick α-In_2Se_3 as the channel, a 20 nm h-BN layer as the top gate dielectric, 30 nm Al_2O_3 as the bottom dielectric layer, and a heavily p-doped silicon substrate as the global gate. Another 20 nm h-BN layer was used between the α-In_2Se_3 layer and the Al_2O_3 for interfacial optimization. The false-colour AFM image of the device is shown in Figure 6h. Ferroelectric semiconducting α-In_2Se_3 features the coexistence of both mobile charges and polarized bound charges. When the α-In_2Se_3-based FeCTs are polarized, positive and negative bound charges are distributed on the upper and lower surfaces of the channel, while the positive and negative mobile charges accumulate on the opposite sides, forming a built-in electric field to maintain the polarization-bound charge. Therefore, FeCTs have a longer retention time and improved endurance of nonvolatile memory. The working mechanism is the same as the FeS-FET, as discussed above. It should be noted that the gate dielectric in the device has a high EOT, resulting in incomplete polarization switching and localized mobile charge distribution. The top gate used does not cover the channel completely, resulting in a weaker polarization that will depolarize in a short time. However, with the accumulation of pulses, a nonvolatile polarization can ultimately be formed. These two processes of volatile and nonvolatile polarization are similar to the neural computing simulations of short-term plasticity (STP) and long-term plasticity (LTP) in biology. Figure 6i shows that, using top gate voltage spikes to stimulate presynaptic input and channel current as postsynaptic current (PSC), with the increase of the spike amplitudes, the PSC exhibits incremental variations in response to the spikes while returning to the initial state quickly, which mimics a typical biological STP. Eventually, the α-In_2Se_3-based FeCTs integrate the nonvolatile memory and computing functions and achieve a 40 ns fast writing speed with a low energy consumption of 234/40 fJ per spike for excitation/inhibition.

α-In_2Se_3 has been mostly used in recent studies on synaptic devices due to its out-of-plane and in-plane polarization coupling, which is suitable for developing multiterminal synaptic devices.[78,99–103] Besides, α-In_2Se_3 has also been further studied in reservoir computing (RC), which is a framework for computation that maps input signals into higher dimensional computational spaces through the dynamics of a fixed non-linear system very recently.[104–106] Compared to other recurrent neural networks, RC benefits from the following two aspects. The first is its low training cost because the training is performed only at the readout stage. Second, the computational cost is low since a variety of naturally physical systems can be used as the reservoir.[107] In addition to α-In_2Se_3, synaptic devices based on other 2D ferroelectrics such as CIPS,[108–110] SnS[56,111] and SnSe[112] have also been demonstrated.

4.4. Ferroelectric Tunnel Junction (FTJ) Devices

An FTJ is a kind of two-terminal vertical heterostructure using a ferroelectric layer as the tunneling barrier with average barrier height (ABH) modified by switching the ferroelectric polarization. The change in ABH results in different tunneling electrore-

sistances (TER).[113] In FTJs based on conventional ferroelectrics, the typical TER ratio ranges from 10 to 10^6,[114] which is limited by a relatively low change in ABH of value below 0.1 eV. In 2020, Wu et al.[113] fabricated an FTJ with a giant TER ratio over 10^7. In the device, they used a 4 nm thick CIPS as the tunneling barrier and graphene and chromium as the asymmetric contacts, as shown in **Figure 7**a. The high TER ratio comes from the giant barrier height modulation up to 1 eV from the ferroelectric doping in graphene. As shown in Figure 7b, the ferroelectric polarization of CIPS dopes graphene from relatively intrinsic to n-type or p-type, resulting in a significant change in the ABH. Such efficient tunnelling barrier height modulation was attributed to the all-vdW nature of the CIPS/graphene interface. Figure 7c shows the I-V characteristics with a high on/off ratio, which was supported by the nonequilibrium Green's function simulation results (the dashed line).[115]

A drawback of CIPS is the relatively low Curie temperature at 315 K compared to other 2D ferroelectrics and conventional oxide ferroelectrics. Therefore, CIPS-based FTJs might suffer device failure due to the thermal effect. Thus, Tang et al.[116] proposed a vdW FTJ device based on α-In_2Se_3, which realizes an on/off ratio of 10^4 at room temperature. Since the T_c of α-In_2Se_3 is ultrahigh, their device still functions normally at a high temperature of 470 K. Similarly, other vdW ferroelectric-based FTJs have also been reported in d$1T$-$MoTe_2$[46] and SnTe.[24]

4.5. Optoelectronic Devices

2D ferroelectric semiconductors are suitable for optoelectronics due to their scalability, clean surfaces, and moderate bandgap. For example, the optoelectronic response of α-In_2Se_3 has been studied for a long time.[117,118] However, it was not until 2019 that its connection to ferroelectricity was established.[25] Among previous optoelectronic studies on conventional ferroelectrics, there is intensive interest in investigating the bulk photovoltaic effect (BPVE), which is a kind of nonlinear optical process that can generate an above-bandgap voltage and exceed the fundamental Shockley-Queisser (S-Q) limit on efficiency.[28,119,120] In 2021, Li et al.[28] reported the enhanced BPVE in 2D ferroelectric CIPS. As shown in Figure 7d, the device was fabricated on a SiO_2/Si substrate employing an ultrathin CIPS layer sandwiched by two layers of graphene as the top and bottom electrodes. The ferroelectric polarizations of CIPS are able to tune the alignment of the energy band and lead to an asymmetric energy potential barrier,[113] as shown in Figure 7e. When illuminated with light, with a broken inversion symmetry, the photogenerated electron and hole pairs will be separated, generating a direction switchable photocurrent (Figure 7f). In addition, the performance of these 2D ferroelectric photovoltaics falls in between the one–dimensional and three–dimensional bulk photovoltaics, implying that the device dimensionality is one of the key factors for developing high-efficiency BPVE-based photovoltaics.

In addition to optoelectronics and photovoltaics, Zha et al.[121] reported RC systems driven by both electrical and optical pulses very recently. Utilizing a metal-ferroelectric-insulator-semiconductor (MFMIS) architecture, in which the semiconducting Te layer serves as the photoactive channel and the ferroelectric CIPS layer is used to introduce memory behavior, they
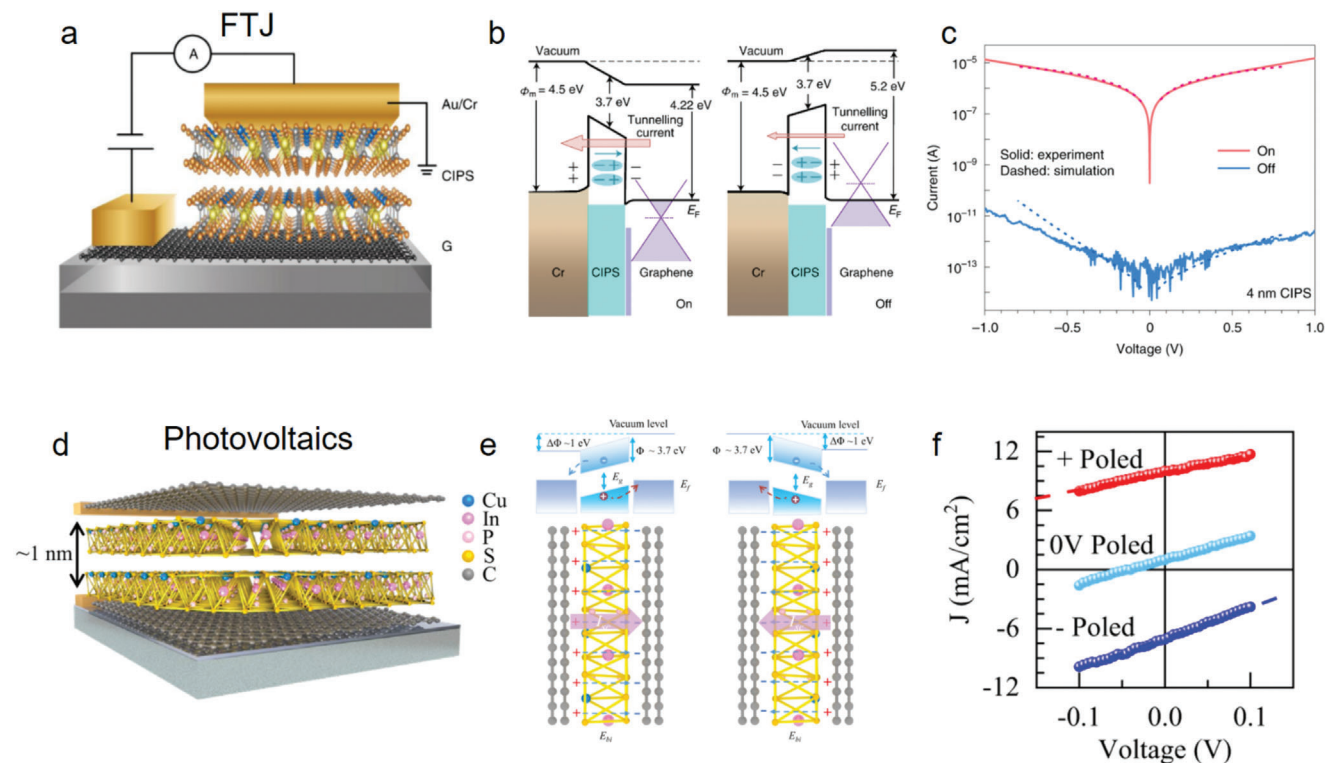
Figure 7. FTJ and photovoltaics based on CIPS. a) Schematic diagram of the Cr/CIPS/graphene FTJ.[113] b) Band diagrams of the FTJ in the on/off state, where cyan arrows represent the built-in polarization field in the CIPS and pink arrows indicate the tunneling current.[113] c) I-V characteristics with an on/off ratio over 10^7.[113] d) Schematic diagram of the 2D BPVE device.[28] e) The band diagrams for the graphene/CIPS/graphene heterostructure at the upwards and downwards electric polarization states and paraelectric phase of CIPS.[28] f) The output I-V curves under different poled states.[28] Reproduced under the terms of the CC–BY license.[28] Copyright 2021, The Authors, published by Springer Nature. Reproduced with permission.[113] Copyright 2020, Springer Nature.

constructed a fully memristive in-sensor RC system that can simultaneously sense, decode, and learn messages transmitted by optical fibers. In addition, a multimode RC system consists of optoelectronic synapses based on α-In_2Se_3 was also reported,[122] showing the potential of α-In_2Se_3-based optoelectronic synapses for developing high-performance computing systems.

5. Summary and Outlook

To summarize, with vast efforts involved in recent years, a consensus has been recognized that atomically thin vdW ferroelectrics are promising candidates for ultimate electronics and optoelectronics in the post Moore era. In addition to robust 2D ferroelectricity, many intriguing features, such as electric-dipole locking, ferroionic coupling, negative piezoelectricity, and enhanced photoresponse, have been revealed. These properties make 2D ferroelectrics an unprecedented platform to explore the interplay between electric polarization and ionic/electronic conductivity, optical excitonic interaction, mechanical flexibility, and superconducting correlation and raise numerous inspirations of novel functional devices beyond physics.

At current stage, 2D ferroelectrics have shown potential applications in nonvolatile memories, neuromorphic devices, photovoltaics, photoelectric detectors, etc. However, there are several challenges that may hinder the future industrial applications of

2D ferroelectric devices. First, although many efforts have been devoted to explore vdW ferroelectrics, only a few 2D intrinsic ferroelectric materials have been experimentally discovered to date, resulting limited material choices for device fabrications. To expand the family of 2D vdW ferroelectrics, more theoretical and experimental efforts are still needed. Second, it is still challenging to obtain large-area and high-quality 2D ferroelectrics at the monolayer limit. The widely used mechanical exfoliation method suffers the issues of limited sample size and yield that fails to meet the demand of manufacturing uniform devices at large scale. It is necessary to develop advanced methods of synthesizing ultrathin 2D ferroelectrics. In addition, the development of large-scale integration processes for efficiently preparing wafer-scale devices and improving the stability of 2D ferroelectric devices will also provide rich research opportunities in various fields. The third challenge in the research field of 2D ferroelectrics might be the universal control of polarizations or ferroelectric domains. There is a need to develop a new method of polarization control beyond electric switching due to the material breakdown problem that originates from their atomic thickness. A recently demonstrated effective method is mechanical switching via the flexoelectric effect.[123,124] The use of mechanical manipulation is completely free from external electric fields, which can avoid the material breakdown problem under the 2D limit.

Conflict of Interest

The authors declare no conflict of interest.

Author Contributions

S.L., G.Z., and Q.L. contributed equally to this work. All authors made important contributions to the review.

[1] J. Valasek, *Phys. Rev.* **1921**, *17*, 475.
[2] O. Auciello, J. F. Scott, R. Ramesh, *Phys. Today* **1998**, *51*, 22.
[3] A. K. Tagantsev, V. O. Sherman, K. F. Astafiev, J. Venkatesh, N. Setter, *J. Electroceramics* **2003**, *11*, 5.
[4] J. F. Scott, *Science* **2007**, *315*, 954.
[5] I. Grinberg, D. V. West, M. Torres, G. Gou, D. M. Stein, L. Wu, G. Chen, E. M. Gallo, A. R. Akbashev, P. K. Davies, J. E. Spanier, A. M. Rappe, *Nature* **2013**, *503*, 509.
[6] Z. Guan, H. Hu, X. Shen, P. Xiang, N. Zhong, J. Chu, C. Duan, *Adv. Electron. Mater.* **2020**, *6*, 1900818.
[7] C. Wang, L. You, D. Cobden, J. Wang, *Nat. Mater.* **2023**, *22*, 542.
[8] P. W. M. Blom, R. M. Wolf, J. F. M. Cillessen, M. P. C. M. Krijn, *Phys. Rev. Lett.* **1994**, *73*, 2107.
[9] Q. Jin, C. Zheng, Y. Zhang, C. Lu, J. Dai, Z. Wen, *Appl. Phys. Lett.* **2017**, *111*, 032902.
[10] T. Hirai, K. Teramoto, K. Nagashima, H. Koike, Y. T. Y. Tarui, *Jpn. J. Appl. Phys.* **1995**, *34*, 4163.
[11] J. Müller, E. Yurchuk, T. Schlösser, J. Paul, R. Hoffmann, S. Müller, D. Martin, S. Slesazeck, P. Polakowski, J. Sundqvist, M. Czernohorsky, K. Seidel, P. Kücher, R. Boschke, M. Trentzsch, K. Gebauer, U. Schröder, T. Mikolajick, in *2012 Symposium on VLSI Technology (VLSIT)*, **2012**, pp. 25–26.
[12] Z. Wen, C. Li, D. Wu, A. Li, N. Ming, *Nat. Mater.* **2013**, *12*, 617.
[13] Q. Yang, L. Tao, Y. Zhang, M. Li, Z. Jiang, E. Y. Tsymbal, V. Alexandrov, *Nano Lett.* **2019**, *19*, 7385.
[14] S. Fujii, Y. Kamimuta, T. Ino, Y. Nakasaki, R. Takaishi, M. Saitoh, in *2016 IEEE Symposium on VLSI Technology*, **2016**, pp. 1–2.
[15] S. Migita, Y. Morita, T. Matsukawa, M. Masahara, H. Ota, *IEEE Trans. Nanotechnol.* **2014**, *13*, 208.
[16] S. B. Desai, S. R. Madhvapathy, A. B. Sachid, J. P. Llinas, Q. Wang, G. H. Ahn, G. Pitner, M. J. Kim, J. Bokor, C. Hu, H. S. P. Wong, A. Javey, *Science* **2016**, *354*, 99.
[17] F. Wu, H. Tian, Y. Shen, Z. Hou, J. Ren, G. Gou, Y. Sun, Y. Yang, T. Ren, *Nature* **2022**, *603*, 259.
[18] D. Ji, S. Cai, T. R. Paudel, H. Sun, C. Zhang, L. Han, Y. Wei, Y. Zang, M. Gu, Y. Zhang, W. Gao, H. Huyan, W. Guo, D. Wu, Z. Gu, E. Y. Tsymbal, P. Wang, Y. Nie, X. Pan, *Nature* **2019**, *570*, 87.
[19] S. S. Cheema, D. Kwon, N. Shanker, R. dos Reis, S.-L. Hsu, J. Xiao, H. Zhang, R. Wagner, A. Datar, M. R. McCarter, C. R. Serrao, A. K. Yadav, G. Karbasian, C.-H. Hsu, A. J. Tan, L.-C. Wang, V. Thakare, X. Zhang, A. Mehta, E. Karapetrova, R. V. Chopdekar, P. Shafer, E. Arenholz, C. Hu, R. Proksch, R. Ramesh, J. Ciston, S. Salahuddin, *Nature* **2020**, *580*, 478.
[20] P. W. Anderson, E. I. Blount, *Phys. Rev. Lett.* **1965**, *14*, 217.
[21] Z. Fei, W. Zhao, T. A. Palomaki, B. Sun, M. K. Miller, Z. Zhao, J. Yan, X. Xu, D. H. Cobden, *Nature* **2018**, *560*, 336.
[22] A. Jindal, A. Saha, Z. Li, T. Taniguchi, K. Watanabe, J. C. Hone, T. Birol, R. M. Fernandes, C. R. Dean, A. N. Pasupathy, D. A. Rhodes, *Nature* **2023**, *613*, 48.
[23] F. Liu, L. You, K. L. Seyler, X. Li, P. Yu, J. Lin, X. Wang, J. Zhou, H. Wang, H. He, S. T. Pantelides, W. Zhou, P. Sharma, X. Xu, P. M. Ajayan, J. Wang, Z. Liu, *Nat. Commun.* **2016**, *7*, 12357.
[24] K. Chang, J. Liu, H. Lin, N. Wang, K. Zhao, A. Zhang, F. Jin, Y. Zhong, X. Hu, W. Duan, Q. Zhang, L. Fu, Q.-K. Xue, X. Chen, S.-H. Ji, *Science* **2016**, *353*, 274.
[25] P. Hou, Y. Lv, X. Zhong, J. Wang, *ACS Appl. Nano Mater.* **2019**, *2*, 4443.
[26] F. Xue, X. He, W. Liu, D. Periyanagounder, C. Zhang, M. Chen, C.-H. Lin, L. Luo, E. Yengel, V. Tung, T. D. Anthopoulos, L.-J. Li, J.-H. He, X. Zhang, *Adv. Funct. Mater.* **2020**, *30*, 2004206.
[27] K. Xu, W. Jiang, X. Gao, Z. Zhao, T. Low, W. Zhu, *Nanoscale* **2020**, *12*, 23488.
[28] Y. Li, J. Fu, X. Mao, C. Chen, H. Liu, M. Gong, H. Zeng, *Nat. Commun.* **2021**, *12*, 5896.
[29] M. Si, P.-Y. Liao, G. Qiu, Y. Duan, P. D. Ye, *ACS Nano* **2018**, *12*, 6700.
[30] S. Wan, Y. Li, W. Li, X. Mao, W. Zhu, H. Zeng, *Nanoscale* **2018**, *10*, 14885.
[31] S. Wan, Y. Li, W. Li, X. Mao, C. Wang, C. Chen, J. Dong, A. Nie, J. Xiang, Z. Liu, W. Zhu, H. Zeng, *Adv. Funct. Mater.* **2019**, *29*, 1808606.
[32] M. Si, A. K. Saha, S. Gao, G. Qiu, J. Qin, Y. Duan, J. Jian, C. Niu, H. Wang, W. Wu, S. K. Gupta, P. D. Ye, *Nat. Electron.* **2019**, *2*, 580.
[33] X. Wang, P. Yu, Z. Lei, C. Zhu, X. Cao, F. Liu, L. You, Q. Zeng, Y. Deng, C. Zhu, J. Zhou, Q. Fu, J. Wang, Y. Huang, Z. Liu, *Nat. Commun.* **2019**, *10*, 3037.
[34] W. Huang, F. Wang, L. Yin, R. Cheng, Z. Wang, M. G. Sendeku, J. Wang, N. Li, Y. Yao, J. He, *Adv. Mater.* **2020**, *32*, 1908040.
[35] S. Baek, H. H. Yoo, J. H. Ju, P. Sriboriboon, P. Singh, J. Niu, J.-H. Park, C. Shin, Y. Kim, S. Lee, *Adv. Sci.* **2022**, *9*, 2200566.
[36] J. Wang, J. B. Neaton, H. Zheng, V. Nagarajan, S. B. Ogale, B. Liu, D. Viehland, V. Vaithyanathan, D. G. Schlom, U. V. Waghmare, N. A. Spaldin, K. M. Rabe, M. Wuttig, R. Ramesh, *Science* **2003**, *299*, 1719.
[37] N. Hur, S. Park, P. A. Sharma, J. S. Ahn, S. Guha, S.-W. Cheong, *Nature* **2004**, *429*, 392.
[38] J. A. Brehm, S. M. Neumayer, L. Tao, A. O'Hara, M. Chyasnavichus, M. A. Susner, M. A. McGuire, S. V. Kalinin, S. Jesse, P. Ganesh, S. T. Pantelides, P. Maksymovych, N. Balke, *Nat. Mater.* **2020**, *19*, 43.
[39] W. Ding, J. Zhu, Z. Wang, Y. Gao, D. Xiao, Y. Gu, Z. Zhang, W. Zhu, *Nat. Commun.* **2017**, *8*, 14956.
[40] C. Cui, W.-J. Hu, X. Yan, C. Addiego, W. Gao, Y. Wang, Z. Wang, L. Li, Y. Cheng, P. Li, X. Zhang, H. N. Alshareef, T. Wu, W. Zhu, X. Pan, L.-J. Li, *Nano Lett.* **2018**, *18*, 1253.
[41] J. Xiao, H. Zhu, Y. Wang, W. Feng, Y. Hu, A. Dasgupta, Y. Han, Y. Wang, D. A. Muller, L. W. Martin, P. Hu, X. Zhang, *Phys. Rev. Lett.* **2018**, *120*, 227601.
[42] L. Li, M. Wu, *ACS Nano* **2017**, *11*, 6382.

ADVANCED
SCIENCE NEWS
www.advancedsciencenews.com

ADVANCED
FUNCTIONAL
MATERIALS
www.afm-journal.de

[43] A. Belianinov, Q. He, A. Dziaugys, P. Maksymovych, E. Eliseev, A. Borisevich, A. Morozovska, J. Banys, Y. Vysochanskii, S. V. Kalinin, *Nano Lett.* **2015**, *15*, 3808.

[44] M. Wu, X. C. Zeng, *Nano Lett.* **2017**, *17*, 6309.

[45] T. Ghosh, M. Samanta, A. Vasdev, K. Dolui, J. Ghatak, T. Das, G. Sheet, K. Biswas, *Nano Lett.* **2019**, *19*, 5703.

[46] S. Yuan, X. Luo, H. L. Chan, C. Xiao, Y. Dai, M. Xie, J. Hao, *Nat. Commun.* **2019**, *10*, 1775.

[47] C. R. Woods, P. Ares, H. Nevison-Andrews, M. J. Holwill, R. Fabregas, F. Guinea, A. K. Geim, K. S. Novoselov, N. R. Walet, L. Fumagalli, *Nat. Commun.* **2021**, *12*, 347.

[48] K. Yasuda, X. Wang, K. Watanabe, T. Taniguchi, P. Jarillo-Herrero, *Science* **2021**, *372*, 1458.

[49] M. Vizner Stern, Y. Waschitz, W. Cao, I. Nevo, K. Watanabe, T. Taniguchi, E. Sela, M. Urbakh, O. Hod, M. Ben Shalom, *Science* **2021**, *372*, 1462.

[50] Y. Wan, T. Hu, X. Mao, J. Fu, K. Yuan, Y. Song, X. Gan, X. Xu, M. Xue, X. Cheng, C. Huang, J. Yang, L. Dai, H. Zeng, E. Kan, *Phys. Rev. Lett.* **2022**, *128*, 067601.

[51] Z. Zheng, Q. Ma, Z. Bi, S. de la Barrera, M.-H. Liu, N. Mao, Y. Zhang, N. Kiper, K. Watanabe, T. Taniguchi, J. Kong, W. A. Tisdale, R. Ashoori, N. Gedik, L. Fu, S.-Y. Xu, P. Jarillo-Herrero, *Nature* **2020**, *588*, 71.

[52] R. Niu, Z. Li, X. Han, Z. Qu, D. Ding, Z. Wang, Q. Liu, T. Liu, C. Han, K. Watanabe, T. Taniguchi, M. Wu, Q. Ren, X. Wang, J. Hong, J. Mao, Z. Han, K. Liu, Z. Gan, J. Lu, *Nat. Commun.* **2022**, *13*, 6241.

[53] M. Wu, X. C. Zeng, *Nano Lett.* **2016**, *16*, 3236.

[54] R. Fei, W. Kang, L. Yang, *Phys. Rev. Lett.* **2016**, *117*, 097601.

[55] S. Cai, Y. Lun, D. Ji, P. Lv, L. Han, C. Guo, Y. Zang, S. Gao, Y. Wei, M. Gu, C. Zhang, Z. Gu, X. Wang, C. Addiego, D. Fang, Y. Nie, J. Hong, P. Wang, X. Pan, *Nat. Commun.* **2022**, *13*, 5116.

[56] Y. Bao, P. Song, Y. Liu, Z. Chen, M. Zhu, I. Abdelwahab, J. Su, W. Fu, X. Chi, W. Yu, W. Liu, X. Zhao, Q.-H. Xu, M. Yang, K. P. Loh, *Nano Lett.* **2019**, *19*, 5109.

[57] K. Chang, F. Küster, B. J. Miller, J.-R. Ji, J.-L. Zhang, P. Sessi, S. Barraza-Lopez, S. S. P. Parkin, *Nano Lett.* **2020**, *20*, 6590.

[58] Z. Guan, Y. Zhao, X. Wang, N. Zhong, X. Deng, Y. Zheng, J. Wang, D. Xu, R. Ma, F. Yue, Y. Cheng, R. Huang, P. Xiang, Z. Wei, J. Chu, C. Duan, *ACS Nano* **2022**, *16*, 1308.

[59] C. Liu, W. Wan, J. Ma, W. Guo, Y. Yao, *Nanoscale* **2018**, *10*, 7984.

[60] W. Song, R. Fei, L. Yang, *Phys. Rev. B* **2017**, *96*, 235420.

[61] B. Xu, H. Xiang, Y. Xia, K. Jiang, X. Wan, J. He, J. Yin, Z. Liu, *Nanoscale* **2017**, *9*, 8427.

[62] D.-D. Xu, R.-R. Ma, A.-P. Fu, Z. Guan, N. Zhong, H. Peng, P.-H. Xiang, C.-G. Duan, *Nat. Commun.* **2021**, *12*, 655.

[63] M. A. Susner, A. Belianinov, A. Borisevich, Q. He, M. Chyasnavichyus, H. Demir, D. S. Sholl, P. Ganesh, D. L. Abernathy, M. A. McGuire, P. Maksymovych, *ACS Nano* **2015**, *9*, 12365.

[64] M. Chyasnavichyus, M. A. Susner, A. V. Ievlev, E. A. Eliseev, S. V. Kalinin, N. Balke, A. N. Morozovska, M. A. McGuire, P. Maksymovych, *Appl. Phys. Lett.* **2016**, *109*, 172901.

[65] S. M. Neumayer, E. A. Eliseev, M. A. Susner, A. Tselev, B. J. Rodriguez, J. A. Brehm, S. T. Pantelides, G. Panchapakesan, S. Jesse, S. V. Kalinin, M. A. McGuire, A. N. Morozovska, P. Maksymovych, N. Balke, *Phys. Rev. Mater.* **2019**, *3*, 024401.

[66] S. Zhou, L. You, A. Chaturvedi, S. A. Morris, J. S. Herrin, N. Zhang, A. Abdelsamie, Y. Hu, J. Chen, Y. Zhou, S. Dong, J. Wang, *Mater. Horiz.* **2020**, *7*, 263.

[67] S. M. Neumayer, L. Tao, A. O'Hara, J. Brehm, M. Si, P.-Y. Liao, T. Feng, S. V. Kalinin, P. D. Ye, S. T. Pantelides, P. Maksymovych, N. Balke, *Phys. Rev. Appl.* **2020**, *13*, 064063.

[68] Y. Lai, Z. Song, Y. Wan, M. Xue, C. Wang, Y. Ye, L. Dai, Z. Zhang, W. Yang, H. Du, J. Yang, *Nanoscale* **2019**, *11*, 5163.

[69] A. Dziaugys, K. Kelley, J. A. Brehm, L. Tao, A. Puretzky, T. Feng, A. O'Hara, S. Neumayer, M. Chyasnavichyus, E. A. Eliseev, J. Banys, Y. Vysochanskii, F. Ye, B. C. Chakoumakos, M. A. Susner, M. A. McGuire, S. V. Kalinin, P. Ganesh, N. Balke, S. T. Pantelides, A. N. Morozovska, P. Maksymovych, *Nat. Commun.* **2020**, *11*, 3623.

[70] S. N. Shirodkar, U. V. Waghmare, *Phys. Rev. Lett.* **2014**, *112*, 157601.

[71] J. W. Park, Y. S. Jung, S. H. Park, H. Choi, Y. S. Cho, *Adv. Opt. Mater.* **2022**, *10*, 2200898.

[72] Y. Zhou, D. Wu, Y. Zhu, Y. Cho, Q. He, X. Yang, K. Herrera, Z. Chu, Y. Han, M. C. Downer, H. Peng, K. Lai, *Nano Lett.* **2017**, *17*, 5508.

[73] F. Xue, W. Hu, K.-C. Lee, L.-S. Lu, J. Zhang, H.-L. Tang, A. Han, W.-T. Hsu, S. Tu, W.-H. Chang, C.-H. Lien, J.-H. He, Z. Zhang, L.-J. Li, X. Zhang, *Adv. Funct. Mater.* **2018**, *28*, 1803738.

[74] H. Hu, Y. Sun, M. Chai, D. Xie, J. Ma, H. Zhu, *Appl. Phys. Lett.* **2019**, *114*, 252903.

[75] X. Xu, T. Zhong, N. Zuo, Z. Li, D. Li, L. Pi, P. Chen, M. Wu, T. Zhai, X. Zhou, *ACS Nano* **2022**, *16*, 8141.

[76] F. Xue, X. He, J. R. D. Retamal, A. Han, J. Zhang, Z. Liu, J.-K. Huang, W. Hu, V. Tung, J.-H. He, L.-J. Li, X. Zhang, *Adv. Mater.* **2019**, *31*, 1901300.

[77] Y. Li, C. Chen, W. Li, X. Mao, H. Liu, J. Xiang, A. Nie, Z. Liu, W. Zhu, H. Zeng, *Adv. Electron. Mater.* **2020**, *6*, 2000061.

[78] L. Wang, X. Wang, Y. Zhang, R. Li, T. Ma, K. Leng, Z. Chen, I. Abdelwahab, K. P. Loh, *Adv. Funct. Mater.* **2020**, *30*, 2004609.

[79] S. Wang, L. Liu, L. Gan, H. Chen, X. Hou, Y. Ding, S. Ma, D. W. Zhang, P. Zhou, *Nat. Commun.* **2021**, *12*, 53.

[80] E. Y. Tsymbal, *Science* **2021**, *372*, 1389.

[81] J. Ji, G. Yu, C. Xu, H. J. Xiang, *Phys. Rev. Lett.* **2023**, *130*, 146801.

[82] B. Xu, J. Deng, X. Ding, J. Sun, J. Z. Liu, *NPJ Comput Mater* **2022**, *8*, 47.

[83] F. Ferreira, V. V. Enaldiev, V. I. Fal'ko, S. J. Magorrian, *Sci. Rep.* **2021**, *11*, 13422.

[84] K. L. Seyler, P. Rivera, H. Yu, N. P. Wilson, E. L. Ray, D. G. Mandrus, J. Yan, W. Yao, X. Xu, *Nature* **2019**, *567*, 66.

[85] K. Tran, G. Moody, F. Wu, X. Lu, J. Choi, K. Kim, A. Rai, D. A. Sanchez, J. Quan, A. Singh, J. Embley, A. Zepeda, M. Campbell, T. Autry, T. Taniguchi, K. Watanabe, N. Lu, S. K. Banerjee, K. L. Silverman, S. Kim, E. Tutuc, L. Yang, A. H. MacDonald, X. Li, *Nature* **2019**, *567*, 71.

[86] C. Jin, E. C. Regan, A. Yan, M. Iqbal Bakti Utama, D. Wang, S. Zhao, Y. Qin, S. Yang, Z. Zheng, S. Shi, K. Watanabe, T. Taniguchi, S. Tongay, A. Zettl, F. Wang, *Nature* **2019**, *567*, 76.

[87] E. M. Alexeev, D. A. Ruiz-Tijerina, M. Danovich, M. J. Hamer, D. J. Terry, P. K. Nayak, S. Ahn, S. Pak, J. Lee, J. I. Sohn, M. R. Molas, M. Koperski, K. Watanabe, T. Taniguchi, K. S. Novoselov, R. V. Gorbachev, H. S. Shin, V. I. Fal'ko, A. I. Tartakovskii, *Nature* **2019**, *567*, 81.

[88] A. Weston, Y. Zou, V. Enaldiev, A. Summerfield, N. Clark, V. Zólyomi, A. Graham, C. Yelgel, S. Magorrian, M. Zhou, J. Zultak, D. Hopkinson, A. Barinov, T. H. Bointon, A. Kretinin, N. R. Wilson, P. H. Beton, V. I. Fal'ko, S. J. Haigh, R. Gorbachev, *Nat. Nanotechnol.* **2020**, *15*, 592.

[89] X. Wang, K. Yasuda, Y. Zhang, S. Liu, K. Watanabe, T. Taniguchi, J. Hone, L. Fu, P. Jarillo-Herrero, *Nat. Nanotechnol.* **2022**, *17*, 367.

[90] A. Weston, E. G. Castanon, V. Enaldiev, F. Ferreira, S. Bhattacharjee, S. Xu, H. Corte-León, Z. Wu, N. Clark, A. Summerfield, T. Hashimoto, Y. Gao, W. Wang, M. Hamer, H. Read, L. Fumagalli, A. V. Kretinin, S. J. Haigh, O. Kazakova, A. K. Geim, V. I. Fal'ko, R. Gorbachev, *Nat. Nanotechnol.* **2022**, *17*, 390.

[91] M. Yankowitz, J. I.-J. Wang, A. G. Birdwell, Y.-A. Chen, K. Watanabe, T. Taniguchi, P. Jacquod, P. San-Jose, P. Jarillo-Herrero, B. J. LeRoy, *Nat. Mater.* **2014**, *13*, 786.

[92] L. Jiang, S. Wang, Z. Shi, C. Jin, M. I. B. Utama, S. Zhao, Y.-R. Shen, H.-J. Gao, G. Zhang, F. Wang, *Nat. Nanotechnol.* **2018**, *13*, 204.

**ADVANCED
SCIENCE NEWS**

www.advancedsciencenews.com

**ADVANCED
FUNCTIONAL
MATERIALS**

www.afm-journal.de

[93] Q. Yang, M. Wu, J. Li, *J. Phys. Chem. Lett.* **2018**, *9*, 7160.

[94] L. Rogée, L. Wang, Y. Zhang, S. Cai, P. Wang, M. Chhowalla, W. Ji, S. P. Lau, *Science* **2022**, *376*, 973.

[95] P. Meng, Y. Wu, R. Bian, E. Pan, B. Dong, X. Zhao, J. Chen, L. Wu, Y. Sun, Q. Fu, Q. Liu, D. Shi, Q. Zhang, Y.-W. Zhang, Z. Liu, F. Liu, *Nat. Commun.* **2022**, *13*, 7696.

[96] T. Jin, J. Mao, J. Gao, C. Han, K. P. Loh, A. T. S. Wee, W. Chen, *ACS Nano* **2022**, *16*, 13595.

[97] X. Wang, C. Zhu, Y. Deng, R. Duan, J. Chen, Q. Zeng, J. Zhou, Q. Fu, L. You, S. Liu, J. H. Edgar, P. Yu, Z. Liu, *Nat. Commun.* **2021**, *12*, 1109.

[98] M. A. Zidan, J. P. Strachan, W. D. Lu, *Nat. Electron.* **2018**, *1*, 22.

[99] F. Xue, X. He, Z. Wang, J. R. D. Retamal, Z. Chai, L. Jing, C. Zhang, H. Fang, Y. Chai, T. Jiang, W. Zhang, H. N. Alshareef, Z. Ji, L.-J. Li, J.-H. He, X. Zhang, *Adv. Mater.* **2021**, *33*, 2008709.

[100] J. Gao, J. Zheng, W. Yu, Y. Wang, T. Jin, X. Pan, K. P. Loh, W. Chen, *SmartMat* **2021**, *2*, 88.

[101] Y. Chen, D. Li, H. Ren, Y. Tang, K. Liang, Y. Wang, F. Li, C. Song, J. Guan, Z. Chen, X. Lu, G. Xu, W. Li, S. Liu, B. Zhu, *Small* **2022**, *18*, 2203611.

[102] Y. Zhai, P. Xie, J. Hu, X. Chen, Z. Feng, Z. Lv, G. Ding, K. Zhou, Y. Zhou, S.-T. Han, *Appl. Phys. Rev.* **2023**, *10*, 011408.

[103] D. Dutta, S. Mukherjee, M. Uzhansky, P. K. Mohapatra, A. Ismach, E. Koren, *ACS Appl. Mater. Interfaces* **2023**, *15*, 18505.

[104] K. Liu, B. Dang, T. Zhang, Z. Yang, L. Bao, L. Xu, C. Cheng, R. Huang, Y. Yang, *Adv. Mater.* **2022**, *34*, 2108826.

[105] N. T. Duong, Y.-C. Chien, H. Xiang, S. Li, H. Zheng, Y. Shi, K.-W. Ang, *Adv Intell Syst* **2023**, 2300009.

[106] J. Y. Yang, M. Park, M. J. Yeom, Y. Baek, S. C. Yoon, Y. J. Jeong, S. Y. Oh, K. Lee, G. Yoo, *ACS Nano* **2023**, *17*, 7695.

[107] G. Tanaka, T. Yamane, J. B. Héroux, R. Nakane, N. Kanazawa, S. Takeda, H. Numata, D. Nakano, A. Hirose, *Neural Netw* **2019**, *115*, 100.

[108] Y. Wang, W. Li, Y. Guo, X. Huang, Z. Luo, S. Wu, H. Wang, J. Chen, X. Li, X. Zhan, H. Wang, *J. Mater. Sci. Technol.* **2022**, *128*, 239.

[109] X. Jiang, X. Wang, X. Wang, X. Zhang, R. Niu, J. Deng, S. Xu, Y. Lun, Y. Liu, T. Xia, J. Lu, J. Hong, *Nat. Commun.* **2022**, *13*, 574.

[110] W. Li, Y. Guo, Z. Luo, S. Wu, B. Han, W. Hu, L. You, K. Watanabe, T. Taniguchi, T. Alava, J. Chen, P. Gao, X. Li, Z. Wei, L.-W. Wang, Y.-Y. Liu, C. Zhao, X. Zhan, Z. V. Han, H. Wang, *Adv. Mater.* **2023**, *35*, 2208266.

[111] K. C. Kwon, Y. Zhang, L. Wang, W. Yu, X. Wang, I.-H. Park, H. S. Choi, T. Ma, Z. Zhu, B. Tian, C. Su, K. P. Loh, *ACS Nano* **2020**, *14*, 7628.

[112] H. Wang, W. Lu, S. Hou, B. Yu, Z. Zhou, Y. Xue, R. Guo, S. Wang, K. Zeng, X. Yan, *Nanoscale* **2020**, *12*, 21913.

[113] J. Wu, H.-Y. Chen, N. Yang, J. Cao, X. Yan, F. Liu, Q. Sun, X. Ling, J. Guo, H. Wang, *Nat. Electron.* **2020**, *3*, 466.

[114] V. Garcia, M. Bibes, *Nat. Commun.* **2014**, *5*, 4289.

[115] D. Zhang, P. Schoenherr, P. Sharma, J. Seidel, *Nat. Rev. Mater.* **2023**, *8*, 25.

[116] W. Tang, X. Zhang, H. Yu, L. Gao, Q. Zhang, X. Wei, M. Hong, L. Gu, Q. Liao, Z. Kang, Z. Zhang, Y. Zhang, *Small Methods* **2022**, *6*, 2101583.

[117] R. B. Jacobs-Gedrim, M. Shanmugam, N. Jain, C. A. Durcan, M. T. Murphy, T. M. Murray, R. J. Matyi, R. L. Moore, B. Yu, *ACS Nano* **2014**, *8*, 514.

[118] J. O. Island, S. I. Blanter, M. Buscema, H. S. J. van der Zant, A. Castellanos-Gomez, *Nano Lett.* **2015**, *15*, 7853.

[119] D. Ouyang, N. Zhang, Y. Li, T. Zhai, *Adv. Funct. Mater.* **2023**, *33*, 2208321.

[120] S. Aftab, M. Z. Iqbal, Z. Haider, M. W. Iqbal, G. Nazir, M. A. Shehzad, *Adv. Opt. Mater.* **2022**, *10*, 2201288.

[121] J. Zha, S. Shi, A. Chaturvedi, H. Huang, P. Yang, Y. Yao, S. Li, Y. Xia, Z. Zhang, W. Wang, H. Wang, S. Wang, Z. Yuan, Z. Yang, Q. He, H. Tai, E. H. T. Teo, H. Yu, J. C. Ho, Z. Wang, H. Zhang, C. Tan, *Adv. Mater.* **2023**, 2211598.

[122] K. Liu, T. Zhang, B. Dang, L. Bao, L. Xu, C. Cheng, Z. Yang, R. Huang, Y. Yang, *Nat. Electron.* **2022**, *5*, 761.

[123] C. Chen, H. Liu, Q. Lai, X. Mao, J. Fu, Z. Fu, H. Zeng, *Nano Lett.* **2022**, *22*, 3275.

[124] W. Ming, B. Huang, S. Zheng, Y. Bai, J. Wang, J. Wang, J. Li, *Sci. Adv.* **2022**, *8*, eabq1232.

[125] M. Wu, J. Li, *Proc Natl Acad Sci U S A* **2021**, *118*, e2115703118.

Shenmao Lin is currently a Ph.D. candidate in the Hefei National Research Center for Physical Sciences at the Microscale at the University of Science and Technology of China. He received a Bachelor's degree in applied physics from University of Science and Technology of China. His research mainly focuses on optoelectronics in two-dimensional materials.
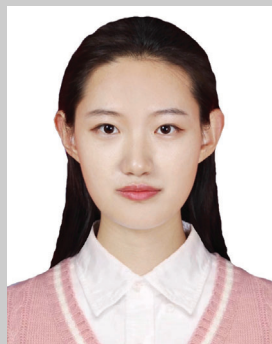
Geyang Zhang is currently a Ph.D. candidate in the Hefei National Research Center for Physical Sciences at the Microscale at the University of Science and Technology of China. She received a Bachelor's degree in physics from Northeast Normal University. Her research mainly focuses on superconductivity in two-dimensional materials.

Qinglin Lai is currently a Ph.D. candidate in the Hefei National Research Center for Physical Sciences at the Microscale at University of Science and Technology of China. She received a Bachelor's degree in applied physics from University of Science and Technology of China. Her research mainly focuses on flexoelectric effect in two-dimensional materials.

Jun Fu is currently a Ph.D. candidate in the Hefei National Research Center for Physical Sciences at the Microscale at the University of Science and Technology of China. He received a Bachelor's degree in physics from Shandong University. His research mainly focuses on nonlinear optics in two-dimensional materials.

Wenguang Zhu is currently a full professor in the School of Physical Sciences at the University of Science and Technology of China. He received a Bachelor's degree from Peking University and a Ph.D. degree in condensed matter physics from the Institute of Physics, Chinese Academy of Sciences. His research mainly focuses on the computational study of low-dimensional functional materials.

**ADVANCED
SCIENCE NEWS**

www.advancedsciencenews.com

**ADVANCED
FUNCTIONAL
MATERIALS**

www.afm-journal.de

Hualing Zeng is currently a full professor in the Hefei National Research Center for Physical Science at the Microscale at the University of Science and Technology of China. He received a Bachelor's degree from the University of Science and Technology of China in 2006 and a Ph.D. degree in condensed matter physics from University of Hong Kong in 2011. His research mainly focuses on the experimental study of two-dimensional semiconductors and ferroelectrics.